

Clustering Time-Snapshots of Temporal Networks: From Synthetic Data to Real-World Applications

Filip Blašković* Tim O.F. Conrad† Stefan Klus‡ Nataša Djurdjevac Conrad§

Abstract

The evolution of many dynamical systems that describe relationships or interactions between objects can be effectively modeled by temporal networks, which are typically represented as a sequence of static network snapshots. In this paper, we introduce a novel random walk based approach that can identify clusters of time-snapshots in which network community structures are stable. This allows to detect significant structural shifts over time, such as the splitting, merging, birth, or death of communities. We also provide a low-dimensional representation of entire snapshots, placing those with similar community structure close to each other in the feature space. To validate our approach, we develop an agent-based algorithm that generates synthetic datasets with the desired characteristic properties, enabling thorough testing and benchmarking. We further demonstrate the effectiveness and broad applicability of our technique by testing it on various social dynamics models and real-world datasets and comparing its performance to several state-of-the-art algorithms. Our findings highlight the strength of our approach to correctly capture and analyze the dynamics of complex systems.

Keywords: Temporal networks, Spectral clustering, Random walk, Benchmark generator, Low-dimensional representation

1 Introduction

Temporal networks, also known as *time-evolving* or *dynamic* networks, can effectively model various complex systems in which entities (represented as nodes or vertices) and the relationships between them (modeled by edges or links) change over time. In contrast to *static networks*, which are useful for representing systems where the relationships are stable, such as electrical or signaling networks [8, 33]; temporal networks take into account the effects of time and offer a more realistic representation of complex systems [25]. In social networks, for instance, the frequency of interactions between individuals may vary across different time periods: for example, colleagues may communicate frequently during work hours, while during weekends or vacations these contacts may decrease. This makes temporal networks an ideal approach for modeling time-dependent behavior. Temporal networks have many applications including neural and brain networks [4, 13], biological ecosystems [2], epidemic spreading [28, 55], and economic scenarios [29].

The analysis of network structure plays a crucial role in understanding the behavior of the underlying complex system. In particular, the identification of *communities* (also called *clusters* or *modules*), which are defined as densely connected groups of nodes, reveals the systems' structural

*Zuse Institute Berlin, Berlin, Germany. blaskovic@zib.de

†Zuse Institute Berlin, Berlin, Germany. conrad@zib.de

‡Heriot-Watt University, Edinburgh, UK. S.Klus@hw.ac.uk

§Zuse Institute Berlin, Berlin, Germany. natasa.conrad@zib.de

and functional organization [47]. Studying how these communities form, dissolve, and transform over time gives valuable insights into the underlying dynamics and interaction patterns [54]. For example, analyzing the network representations of the human microbiome and its microbial communities helps us understand how diseases or medical treatments impact these systems and the nature of the resulting disturbances [43]. The human microbiome, which typically maintains a stable equilibrium, can be significantly changed following the onset of disease. In network terms, during healthy periods, microbial groups interact intensively between their members and form communities in the network. However, when the individual becomes ill, these interactions within the existing communities decrease, while interactions among other microbial groups increase, leading to a new stable structural configuration in the network. In Figure 1, we show a simplified illustration of this process, where we consider a temporal network to be a sequence of static networks over a discretized time interval $[0, 20]$. Initially, the network features two communities (snapshots 0 to 10) corresponding to the "healthy" state and as the network evolves, one community splits into two smaller ones, leading to a new stable structural configuration (snapshots 11 to 20) that describes an "ill" state.

Despite recent advances in the field, the identification of communities in temporal networks and tracking their evolution over time remains a challenging problem [54], particularly when dealing with large-scale and noisy datasets coming from real-world systems. To address this challenge we propose a method that clusters time-snapshots into so-called *phases*, during which network communities remain largely unchanged. Each phase represents a stable network configuration, while transitions between different phases capture important changes in the network’s community structure. Identification of phases allows to significantly reduce the computational cost of performing community detection in every single snapshot. Instead, for every phase, we analyze only one (representative) snapshot or alternatively a (weighted) aggregated network obtained from all other snapshots of that phase. In the community dynamics of a temporal network shown in Figure 1, we can distinguish between two phases: a "healthy" phase with two communities (snapshots 0 to 10), and an "ill" phase with three communities (snapshots 11 to 20).

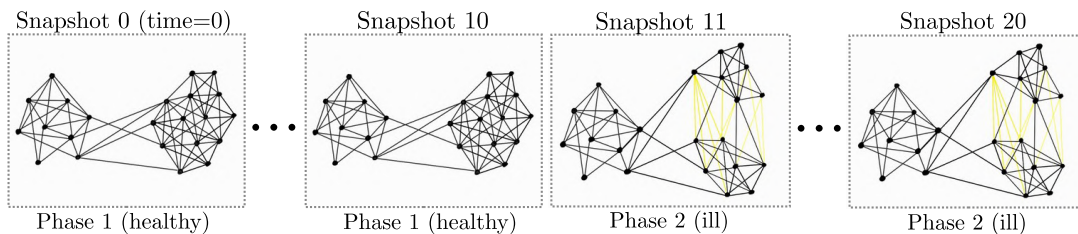


Figure 1: A temporal network with two phases. At the 11th time step, the right community splits into two, marking the transition between the phases. The yellow edges in snapshots 11 to 20 represent edges that are not present anymore after the transition. Our new method can correctly identify the two phases and the time when the change occurred, and find a low-dimensional embedding of the snapshots.

In this work, we introduce a novel random walk-based approach that captures similarity between community structures of networks from different snapshots. We consider independent *spatial random walks* on each of the snapshots to analyze their community structure and obtain transition matrices. Our method uses the property that network communities are encoded in the block structure of the transition matrix. Thus, by comparing transition matrices of networks from different snapshots, we can detect changes in the communities over time. To quantify this, we introduce a measure of

similarity between snapshots, such that snapshots with (almost) the same community structure have high similarity and snapshots with very different community structure have low similarity. We use these values to introduce a new static network, where nodes correspond to snapshots of the temporal network and we define edge strengths between these nodes using the snapshot similarity. This new network serves as a reduced model of the original temporal network and it encodes information about phases of the temporal network. That is, nodes corresponding to the snapshots of the same phase will be densely connected by edges with large weights and form a community within the reduced model, while snapshots with very different communities will be weakly connected. Finally, we define a *temporal random walk process* on this new static network and use spectral clustering to identify its communities, i.e., phases of the original temporal network. In Figure 2, we show a schematic illustration of our method, which consists of applications of the two distinct random walk processes mentioned above: a spatial random walk and a temporal random walk.

Additionally, our approach extends the concept of spatio-temporal exploration by introducing time-continuous random walks for both types of processes. This incorporates a time resolution parameter that can regulate the method’s sensitivity to detect variations in community structure and enable phase detection across multiple scales, from fine-grained to coarse-grained resolutions. Similar concepts of spatio-temporal exploration for temporal clustering have been considered in previous work [19, 58, 59, 16]. However, the networks produced in these approaches can become exceptionally large when dealing with a high number of nodes and many snapshots, resulting in significant computational costs for their analysis. In contrast, our method ensures that the size of the reduced model remains independent of the node set size, making it more suitable for larger datasets, often coming from real-world systems. To further support the efficacy of our method, we introduce a new benchmark generator for producing synthetic temporal network data using an agent-based approach. This generator is essential for testing our proposed method under controlled conditions. Synthetic datasets generated with this method form a robust foundation for evaluating our approach and comparing it with other methods.

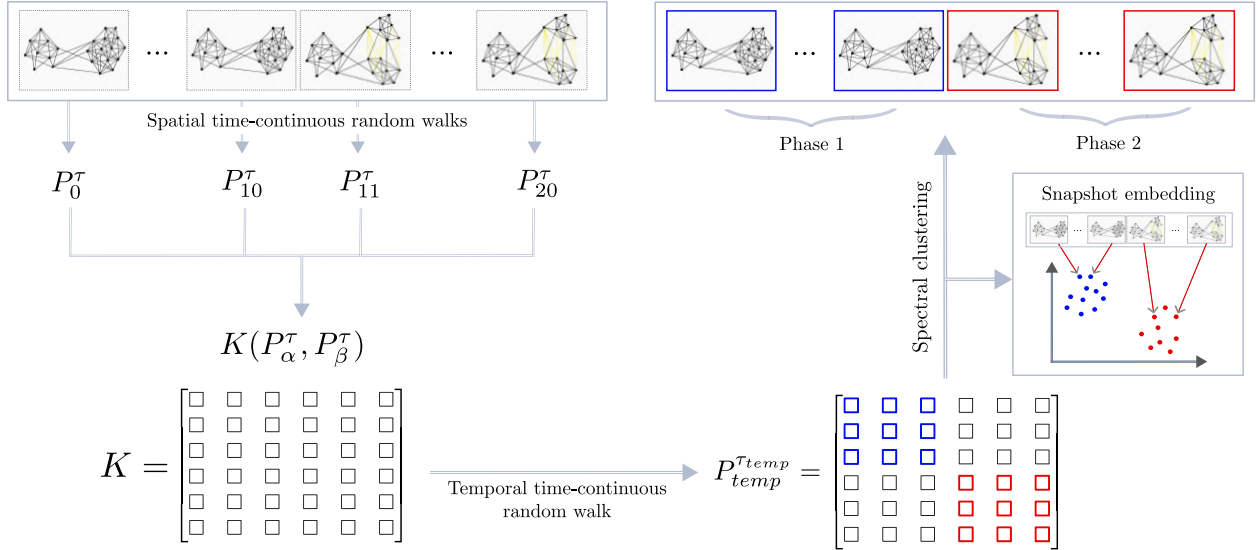


Figure 2: A schematic illustration of our method. First, we independently compute transition matrices of spatial random walks for each snapshot. We then perform pairwise comparisons between the snapshots using an appropriate similarity measure k . Finally, we construct a temporal transition matrix, apply spectral clustering to identify phases, and obtain low-dimensional representations of entire snapshots.

The key contributions of our work are:

- i) We **introduce a new method that can identify phases in temporal network**, i.e., periods of stability within network communities. Our method effectively detects moments when significant community changes occur, such as the splitting, merging, birth, or death of communities. Additionally, we find **low-dimensional embedding of network snapshots** that preserves the similarity between their underlying community structures, enabling effective comparison and analysis across time. Compared to other approaches, our method reduces computational costs, making it more efficient for analyzing large-scale temporal networks.
- ii) We present a **novel benchmark generator** based on an agent-based model to test and validate our approach across various temporal network scenarios. Our benchmark generator is highly versatile and has the potential to be used for evaluating similar methods. This adaptability is crucial, as there is a growing need for standardized benchmarks to evaluate and compare different methods for analyzing temporal networks.

Our paper is structured as follows: We first introduce our novel method for clustering network snapshots in Section 2. Then, in Section 3, we present a short overview of existing benchmark algorithms, introduce a new benchmark generator, and validate our method using the synthetic networks obtained in this way. We continue the validation in Section 4 by applying our method to networks derived from social dynamics models and real-world datasets, showcasing its practical applicability and versatility across different domains. To situate our work within the existing body of research, Section 5 offers an overview of related work alongside a comparative analysis. We examine existing approaches, highlighting how our method not only addresses current gaps but also demonstrates superior performance, thereby underscoring its contributions to the field of dynamic network analysis. Finally, in Sections 6 and 7 we present a brief discussion and conclusion and suggest further research directions.

2 A Novel Method for Clustering Time-Snapshots in Temporal Networks

In this section, we present our new method *Local Neighborhood Exploration (LNE)* and its special case *Invariant Measure Comparison (IMC)*. We illustrate its key steps and capabilities with a guiding example on a synthetic temporal network, demonstrating how it identifies transitions and clusters snapshots based on their community structures.

2.1 Random Walks on Networks

We consider a temporal network $\mathbb{G} = (G_0, \dots, G_{M-1})$ to be a sequence of static networks $G_\alpha = (V_\alpha, E_\alpha)$ at discrete times $\alpha \in \{0, \dots, M-1\}$, given by a set of nodes V_α and a set of edges E_α . We assume that the set of nodes $V_\alpha = V$ is fixed during the entire evolution and that additionally networks in all snapshots are connected, aperiodic and undirected. Let A_α denote the (potentially weighted) adjacency matrix of a snapshot G_α , where $A_\alpha(u, v) = w_\alpha(u, v)$ is the weight of the edge between nodes u and v (if the networks are unweighted, then $w_\alpha(u, v) = 1$ if $(u, v) \in E_\alpha$ and $w_\alpha(u, v) = 0$ otherwise). A standard discrete-time random walk process is defined by a Markov chain with the transition matrix $P_\alpha = [p_\alpha(u, v)]_{u, v \in V}$, given by

$$p_\alpha(u, v) = \frac{A_\alpha(u, v)}{d_\alpha(u)}, \quad \text{with } d_\alpha(u) = \sum_{v \in V} A_\alpha(u, v), \quad (1)$$

where $d_\alpha(u)$ is the (weighted) degree of a node u in a snapshot α . This means that at each time step the random walk process moves to one of the neighboring nodes that has been chosen randomly proportional to the edge weights. From a network perspective, communities are subsets of nodes, where nodes of the same community are densely connected to each other and sparsely connected to nodes in other communities. From a dynamic perspective, communities can be understood as metastable sets of the random walk process [14, 56, 30, 57], i.e., sets of nodes where the process remains “trapped” for a relatively long time before transitioning elsewhere. The community structure of the network is reflected in the long-term behavior of the random walk process. More precisely, for metastable sets $A, B \subset V$, it holds that

(a) the residence probability in a metastable set A is close to 1, i.e., $p_\alpha(A, A) = \mathbb{P}[X_T \in A \mid X_0 \in A] \approx 1$,

(b) the transition probability between A and B is small, i.e., $p_\alpha(A, B) = \mathbb{P}[X_T \in B \mid X_0 \in A] \ll 1$,

for large enough T . The best full partition of the network G_α into $C_\alpha^1, \dots, C_\alpha^k$ disjoint communities, where $\bigcup_{i=1}^k C_\alpha^i = V$ and $C_\alpha^i \cap C_\alpha^j = \emptyset, \forall i \neq j$, is the one that maximizes the joint metastability of the sets

$$\mathcal{D}(C_\alpha^1, \dots, C_\alpha^k) = \sum_{i=1}^k p_\alpha(C_\alpha^i, C_\alpha^i).$$

Since the networks we consider are connected and aperiodic, the random walk process under consideration is ergodic [14]. For ergodic processes, relations between a decomposition into metastable sets and spectral properties of the transition matrix P have been established and used in many spectral clustering algorithms [61]. In particular, the number of metastable sets (communities) can be inferred from the number of dominant (largest) eigenvalues of P and decomposing dominant eigenvectors using their sign structure leads to the identification of these communities [61, 56]. The long-term behavior of the process is encoded in the left eigenvector corresponding to the unique, largest eigenvalue equal to 1. This follows from the fundamental theorem of Markov chains, stating that every ergodic random walk process always converges to the unique *invariant measure* (or stationary distribution) $\tilde{\mu}_\alpha$, where $\tilde{\mu}_\alpha P_\alpha = \tilde{\mu}_\alpha$, i.e., $\tilde{\mu}_\alpha$ is the left eigenvector corresponding to the largest eigenvalue of P_α .

However, it is important to note that not all metastable sets of a random walk correspond to community structures within a network. Other configurations, such as long chains, can also trap the random walk process for extended periods, but do not represent true network communities [14]. To address this, we use time-continuous Markov processes (or Markov jump processes), as introduced in Sarich et al.[56], and for each network snapshot G_α at time α , we introduce a time-continuous random walk process by defining a rate matrix

$$L_\alpha(u, v) = \begin{cases} -\frac{1}{d_\alpha(u)}, & u = v, \\ \frac{A_\alpha(u, v)}{d_\alpha(u)^2}, & u \neq v, (u, v) \in E_\alpha, \\ 0, & \text{otherwise.} \end{cases} \quad (2)$$

Unlike standard discrete-time random walks (see Eq. (1)), this process has the advantage that it incorporates waiting times at each node. Specifically, the expected waiting time at a node u is proportional to its degree $d_\alpha(u)$, allowing the process to move more quickly through loosely connected regions while slowing down and taking longer in densely interconnected structures, i.e., communities. This approach enhances the metastability of communities, thereby improving the performance of traditional spectral methods. For other examples of time-continuous random walk processes we refer to Djurdjevac [14] and Sarich et al.[56]

2.2 Neighborhood Exploration using Random Walks: Spatial Random Walks

The rate matrix L_α is also called the infinitesimal generator of a Markov process, since for a spatial exploration time $\tau > 0$ it can generate the whole family of transition matrices

$$P_\alpha^\tau = \exp(L_\alpha \tau). \tag{3}$$

Efficient computation of the matrix exponential is possible using methods such as Krylov subspace techniques (since L_α is sparse in most applications), making the approach scalable even for large networks. The transition matrix P_α^τ gives the probabilities of a process transitioning between two nodes after the time τ , that is $P_\alpha^\tau = [p_\alpha^\tau(u, v)]$, where $p_\alpha^\tau(u, v) = \mathbb{P}[X_\tau = v \mid X_0 = u]$. The choice of the time parameter τ , which we refer to as *spatial exploration time*, has a significant influence on the behavior of the process, and thus on the spectral properties of P_α^τ and community identification. If τ is small, the random walk process explores only the immediate neighborhood and the transition probabilities reflect the local structure via short-range connections. If τ is large, on the other hand, the process has more time to explore the network and reflects its global long-term behavior such as metastability. Thus, the spectrum of P_α^τ changes with the choice of the spatial exploration time and the optimal choice of τ depends on the desired resolution of the process. Of interest are large (but not too large) values of τ since these may reveal the underlying community structure. If there are k communities (metastable sets) in the network, then the k dominant (largest) eigenvalues $0 = \Lambda_0^\alpha > \Lambda_1^\alpha \geq \dots \geq \Lambda_{k-1}^\alpha$ of L_α are close to zero and are separated by a spectral gap from the smaller eigenvalues. The implied timescales of this process are given by $1/|\Lambda_i^\alpha|$ for $i \geq 1$, and provide bounds for a good choice of τ . Namely, the chosen resolution of the process reflects the granularity of a network[56], so that for finding the k most metastable sets τ should be $1/|\Lambda_k^\alpha| < \tau < 1/|\Lambda_{k-1}^\alpha|$.

Since random walk processes explore the neighborhood of a node for a fixed τ , which results in a constrained exploration range, we will call our method *Local Neighborhood Exploration* (LNE). The LNE method uses transition matrices P_α^τ as effective encodings for comparing community structure across snapshots. For a suitably chosen τ , nodes that belong to communities exhibit a block structure in the transition matrix, potentially after an appropriate permutation of nodes. This comes as a consequence of the metastable behavior of the dynamics within communities: τ is chosen to be small enough so that the random walk does not leave the community due to its metastability, yet large enough to allow the process to sufficiently explore the host community. Thus, on a scale within the community, the probability distribution of the process’s endpoint is approximately the same, regardless of the starting node. Specifically, let G_0 and G_1 be two snapshots, and u, v two nodes belonging to the same community $C \subset V$ that does not change in both snapshots. Then, $P_0^\tau(u, \cdot) \approx P_1^\tau(v, \cdot)$, where $P(u, \cdot)$ denotes the u th row of the matrix P . Hence, the communities accurately correspond to blocks in transition matrices and the stability in the community structures across snapshots is reflected in the similarity of the corresponding transition matrices.

2.3 Guiding Example

As a guiding example, we consider a temporal network $\mathbb{G} = (G_0, \dots, G_{19})$ consisting of 200 nodes and 20 snapshots. The first ten snapshots are formed based on the static network “Phase 1” shown in Figure 3. This network contains 8 distinct communities as highlighted in the figure with different community colors. Each snapshot from 0 to 9 is then obtained by introducing noise through the random addition and deletion of edges within communities in the base network, representing the first phase of the temporal network. Then, at time $\alpha = 10$ new edges are introduced between selected pairs of communities causing them to merge and resulting in the new base network, “Phase 2”, with 5 communities. Snapshots 10 to 19 are now similarly formed by adding noise to this static network

representing the second phase. Figure 3 shows the ten largest eigenvalues of the generator L for the base network of Phase 1 and the base network of Phase 2, revealing spectral gaps after the 8th and 5th eigenvalue, respectively. To accurately detect network communities in both phases, we choose τ from the interval $1/0.014 \approx 70 \leq \tau \leq 250 = 1/0.004$, which is contained in both spectral gaps. In Figure 3 we show the 13 largest eigenvalues (blue crosses) corresponding to the time-continuous random walk of length $\tau = 100$ for both phases and the 13 largest eigenvalues corresponding to the standard random walk (orange circles). We observe that the standard random walk, unlike the continuous approach, fails to capture the community structure, showing no clear spectral gaps, highlighting the higher generalizability of the continuous approach. Furthermore, it is important to note that adjusting the parameter τ modifies the resolution at which communities are detected. In order to keep a consistent resolution during the entire network evolution, we fix the granularity of our algorithm by choosing the same lag time τ for all snapshots.

2.4 Exploring the Long-term Behavior of Random Walks

If the network exploration by the random walk process is performed for a sufficiently long period, then the probability of being at any node is approximately given by the invariant measure. As a special case of the LNE approach, we consider a *Invariant Measure Comparison (IMC)*, where we use the long-term probabilities given by the invariant measure to study network community dynamics. The invariant measure of a time-continuous random walk associated with an infinitesimal generator L_α is a probability distribution μ_α such that $\mu_\alpha L_\alpha = 0$. For a generator matrix defined as in Eq. (2) it can be directly shown that μ_α is given by

$$\mu_\alpha(u) = \frac{1}{Z} d_\alpha(u)^2,$$

where Z is a normalization constant[56]. Since the vector μ_α can be calculated directly using the node degrees, IMC offers a reduction of the computational cost compared to LNE, where additional steps for obtaining the transition matrices and matrix comparison are needed.

The IMC approach is capable of detecting changes in the community structure, as it tracks how the invariant measure of community nodes adapts in response to structural changes in the network. As communities are metastable sets of a random walk process, the probability of finding a random walker within a community is in general higher than being outside of it. When the sizes of the communities change over time, e.g., due to a growth or a shrinkage process, the average invariant measure of community nodes also changes. However, since the invariant measure depends exclusively on node degrees, its ability to capture dynamic network community structure is constrained by the limited information available. For example, if despite the structural change, clusters stay similar in size and density of connections, the IMC method may have difficulties detecting these structural changes. This may be improved in some cases by considering different types of random walk processes [14]. Nevertheless, very often the invariant measure data contains sufficient information for our task. It is particularly suitable for datasets with significantly different cluster sizes and node degree distributions in different phases. Since IMC offers a significant reduction in the algorithm’s complexity compared to LNE, we will consider it as a special case of LNE and test it on different datasets. In Figure 5a we plot the invariant measure within the two phases of the guiding example and observe that communities are easily detectable in the invariant measure values. When communities change their size, e.g., through merging or splitting, the number of connections within them usually changes, and so does the invariant measure. This is often sufficient to capture the key events that lead to shifts in community structure.

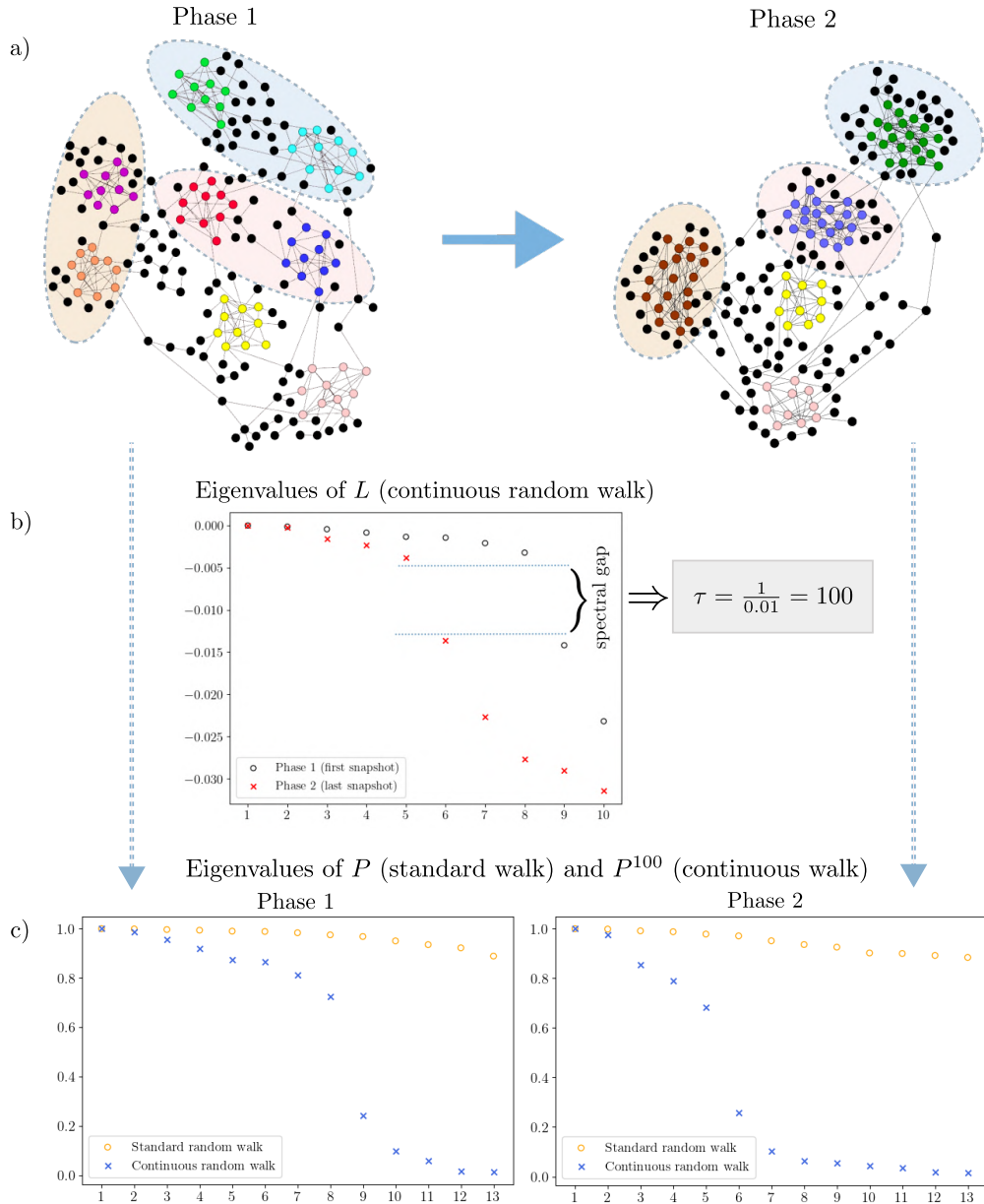


Figure 3: Illustration of the temporal network introduced in the guiding example (see Section 2.3). a) Base networks and their communities for Phase 1 and Phase 2. Nodes colored in black do not belong to any communities. Other node colors indicate the community affiliation. Circled groups of nodes in Phase 1 indicate which communities will merge in the next phase. b) The dominant eigenvalues of the generator L for the base network of Phase 1 (in blue) and Phase 2 (in red). c) The dominant eigenvalues of the transition matrices for both phases, corresponding to the standard (orange circles) and time-continuous (blue crosses) random walks. Note that while eigenvalues are shown here for illustration, our proposed methods do not rely on their explicit computation.

2.5 Clustering of Time-Snapshots in Temporal Networks: Temporal Random Walk

In the previous subsection, we introduced transition matrices and invariant measures as objects that can capture crucial information about the internal structure of each time snapshot. Next, our goal is to identify phases during which the global network structure – particularly the communities within snapshots – remains largely stable. To achieve this, we employ another time-continuous random walk process at a temporal level, where the random walk transitions are between snapshots and not within them. We define a similarity measure between snapshots by using the Gaussian kernel k , which is the standard choice in many applications, although other options are possible[48]. The Gaussian kernel k is defined by:

$$k(P_\alpha^\tau, P_\beta^\tau) = \exp\left(\frac{-\|P_\alpha^\tau - P_\beta^\tau\|_F^2}{2\sigma^2}\right). \quad (4)$$

The parameter σ is called the *bandwidth*. The bandwidth determines the scale of strong relations between snapshots, setting the range within which transition matrices are considered similar. Using these snapshot similarity values, we construct a new static network where nodes represent snapshots and edge weights $K(\alpha, \beta) := k(P_\alpha^\tau, P_\beta^\tau)$ reflect the similarity between their community structures. This network serves as a reduced model of the initial temporal network. Similarly to Eq. (2) we define a *temporal generator matrix* L_{temp} on this new reduced network. In this matrix, the jump rate from snapshot α to snapshot β is given by

$$L_{temp}(\alpha, \beta) = \begin{cases} -\frac{1}{d(\alpha)}, & \alpha = \beta, \\ \frac{K(\alpha, \beta)}{d(\alpha)^2}, & \alpha \neq \beta, \end{cases} \quad (5)$$

where $d(\alpha)$ is the (weighted) degree of a node α . By selecting an appropriate *temporal exploration parameter* τ_{temp} , with respect to the spectral gap of L_{temp} , we obtain the temporal transition matrix $P_{temp}^{\tau_{temp}}$. If multiple spectral gaps are present, different choices of τ_{temp} allow us to fine-tune the sensitivity of our method when grouping snapshots. Smaller values of τ_{temp} make the method more sensitive to subtle variations in communities, while larger values filter out milder changes, requiring more substantial differences for phase change detection. In Figure 4(a-d), we show the results of applying these steps on a network from the guiding example (see Section 2.3). Next, we use spectral clustering to group snapshots with consistent community structure into s phases [61], by computing the matrix $U \in \mathbb{R}^{M \times s}$, whose columns are the eigenvectors corresponding to the dominant eigenvalues of the temporal transition matrix. Finally, we apply k -means clustering to the rows of U to detect these phases. The dominant eigenvectors provide low-dimensional embeddings for the snapshots, where snapshots from the same phase are positioned closely in the feature space (Figure 4e). Since the first eigenvector is constant and adds no variation to the embeddings, it is typically excluded from the procedure. These embeddings are valuable for further temporal network analysis or as input for various machine learning algorithms. Our algorithm is one of the few that can find entire snapshot representations. We will compare its efficacy with alternative methods in Section 5. It is worth noting that the eigenvalue computation for the temporal generator matrix $L_{temp} \in \mathbb{R}^{M \times M}$ is computationally efficient to handle in most practical cases. However, this step could become challenging if an unusually large number of snapshots is considered. For typical applications, M is small enough that this is not a limiting factor.

As an illustration of the results of our algorithm, we show the distance matrix $S \in \mathbb{R}^{M \times M}$ (Figure 4f), whose entries are defined to be distances between rows of matrix U :

$$S(\alpha, \beta) = \frac{1}{Z} \|U(\alpha, :) - U(\beta, :)\|,$$

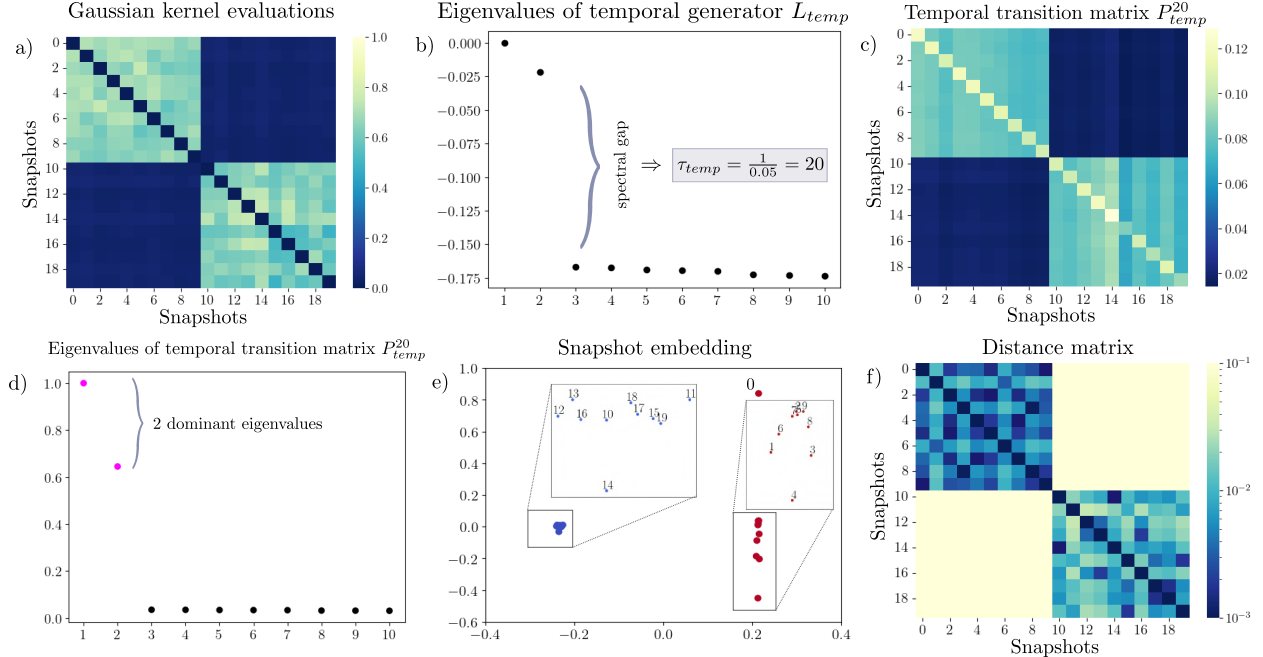


Figure 4: Results of the LNE method applied to the guiding example (see Section 2.3). a) Similarity measures between snapshots, derived from Gaussian kernel evaluations between spatial transition matrices. b) Eigenvalues of the temporal generator L_{temp} . c) Temporal transition matrix P_{temp}^{20} . d) Dominant eigenvalues of P_{temp}^{20} . e) Low-dimensional embedding of entire snapshots partitioned into phases. f) Distance matrix between the rows of matrix U .

where Z is a suitable scaling parameter. The matrix S is expected to exhibit a near-block structure, with low-value blocks along the main diagonal, indicating closely related snapshots with respect to the chosen kernel. This reflects periods of stability within communities during the evolution of the network.

The IMC algorithm is implemented in a similar way, except that we compute $k(\mu_\alpha, \mu_\beta)$ instead of Eq. (4). By omitting computations of Eq. (2) and Eq. (3), this approach achieves greater computational efficiency, although at the cost of some versatility. Figure 5 illustrates the IMC method applied to the guiding example (see Section 2.3). In this example, both LNE and IMC methods effectively capture the two phases of network evolution, as reflected in the block structure of their respective distance matrices.

Remark 2.1 *Note that even though multiple network similarity measures for clustering snapshots have been proposed in the literature [40], we focus here specifically on comparing snapshots based on their community structure. For example, widely used adjacency matrix-based similarity measures would not be appropriate for this task. Namely, the same set of nodes in two snapshots may exhibit completely different internal wiring patterns such that subnetworks spanning the same node subset could even be complementary, yet still form densely interconnected regions in both snapshots. In this case, the adjacency matrices would differ significantly, even though overall community structure remains unchanged. Our approach overcomes this issue and effectively identifies consistent communities across snapshots, despite the variations in their internal connections.*

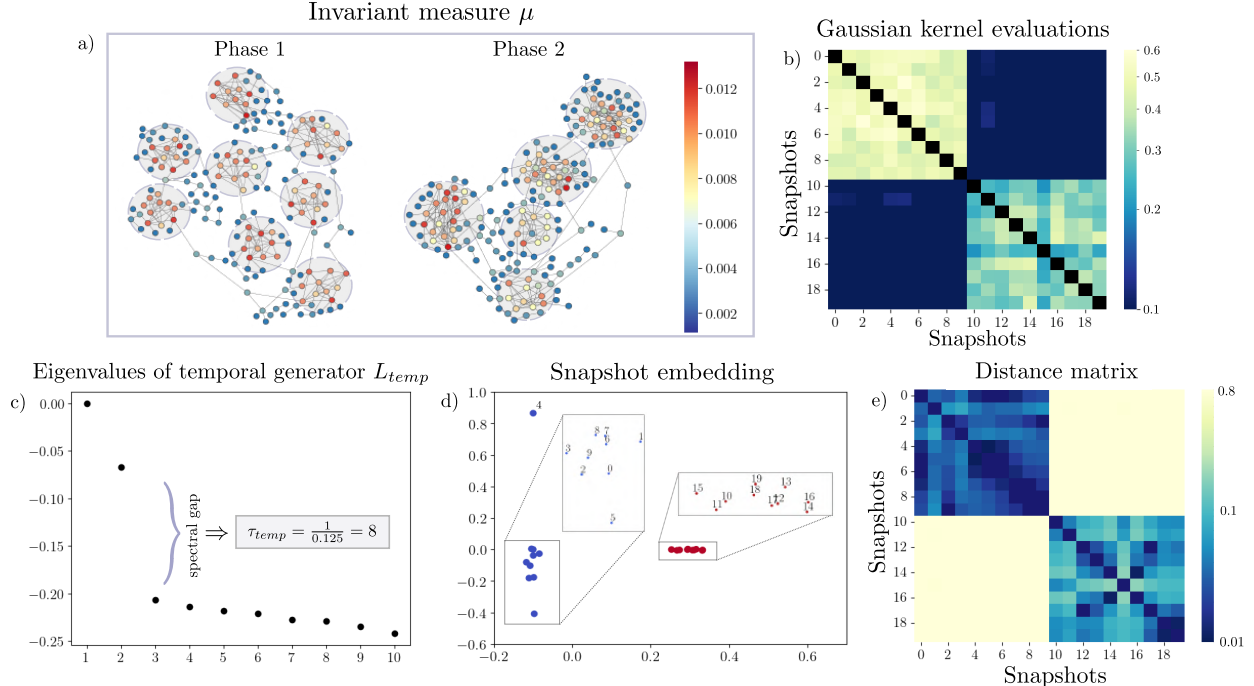


Figure 5: Results of the IMC method applied to the guiding example (see Section 2.3). a) Invariant measure values in base networks. b) Similarity measures between snapshots, derived from Gaussian kernel evaluations between invariant measures. c) Eigenvalues of the temporal generator L_{temp} . d) Low-dimensional embedding of entire snapshots partitioned into phases. e) Distance matrix between the rows of matrix U .

2.6 Identification of Phases of Temporal Networks: Algorithmic considerations

Our approach consists of two main steps:

- (1) we encode snapshots as transition matrices of time-continuous spatial random walks for a suitably chosen τ ;
- (2) we define a time-continuous temporal random walk across snapshots for a suitably chosen τ_{temp} . Using spectral clustering, we then group these snapshots into phases of community stability.

Rather than explicitly computing the spectral decomposition of the generators for each snapshot, which is a computationally intensive task, we can select τ heuristically, based on properties of the dataset, such as the average node degree, as the expected waiting time before a continuous random process takes a new step is proportional to it. However, other factors, such as edge density within communities, size of communities or irregular structural patterns, may also affect the optimal spatial exploration time and should be considered when setting τ . In our experiments on real-world and social dynamics simulation datasets, we heuristically chose τ and then verified that this choice aligns with the relevant spectral gap of the generators L_α . In all examples, we choose τ_{temp} based on the spectral gap of the generator L_{temp} .

The LNE algorithm is summarized in the following pseudo-code:

Algorithm 1 Local Neighborhood Exploration (LNE)

- 1: **Input:** adj – array of adjacency matrices of a temporal network (alternatively: adjacency lists, incidence matrices), τ – spatial exploration time, σ – bandwidth parameter.
 - 2: **for** $\alpha = 0, 1, \dots, M - 1$ **do**
 - 3: Compute L_α and P_α^τ using Eq. (2) and Eq. (3).
 - 4: **end for**
 - 5: Initialize empty matrix K of size $M \times M$.
 - 6: **for** $\alpha = 0, 1, \dots, M - 1$ **do**
 - 7: **for** $\beta = 0, 1, \dots, M - 1$ **do**
 - 8: Set $K(\alpha, \beta) := k(P_\alpha^\tau, P_\beta^\tau) = \exp\left(\frac{-\|P_\alpha^\tau - P_\beta^\tau\|_F^2}{2\sigma^2}\right)$.
 - 9: **end for**
 - 10: **end for**
 - 11: Compute L_{temp} using Eq. (5) for a weighted network with weights given by K . Determine τ_{temp} from the spectral gap of L_{temp} .
 - 12: Compute $P_{temp}^{\tau_{temp}}$.
 - 13: **Apply spectral clustering on** $P_{temp}^{\tau_{temp}}$:
 - 14: Define $U \in \mathbb{R}^{M \times s}$ whose columns are s dominant eigenvectors of $P_{temp}^{\tau_{temp}}$.
 - 15: Run k -means on rows of the matrix U .
 - 16: Assign the labels to the corresponding snapshots and group them.
-

Remark 2.2 *In this work, we compare all possible pairs of snapshots. To reduce the computational complexity, we could also consider a fixed-length sliding window and compute the similarity only between the snapshots within that window. However, this alternative approach would be more sensitive to the occurrence of irregular snapshots (outliers) and would not allow for detecting repeating phases in the network dynamics.*

3 Experiments on Synthetic Data

Creating and analyzing temporal networks in real-world scenarios present significant challenges, including the time and costs required for data collection and privacy constraints. As a result, relying solely on real-world data for method development and validation is often impractical. Synthetically generated networks provide a valuable alternative, offering a controlled and adaptable testing environment. A well-designed synthetic network generator not only captures the essential dynamics of real-world systems but also allows for the creation of networks with diverse characteristics. This flexibility enables rigorous testing, iterative refinement, and validation of methods in an efficient and reliable manner.

In this section, we first provide an overview of existing benchmark networks and then introduce our novel agent-based temporal network generator for method validation. While existing benchmarks employ various mathematical techniques to emulate real-world dynamics, they are often limited to specific properties or lack flexibility to handle high noise levels and complex behaviors. Our agent-based generator addresses these gaps by offering a versatile approach to simulate diverse scenarios, including community formation, evolution, and metastability in temporal networks. Drawing on well-established agent-based modeling techniques, which are widely used in fields such as social dynamics, disease spreading, and economic systems, our generator creates realistic and adaptable synthetic datasets for robust network analysis.

3.1 Overview of Existing Benchmark Networks

Community detection in networks is a multifaceted problem that spans diverse applications, from social networks to biological systems. The diversity and complexity of these systems has driven the development of various benchmarks to evaluate and compare community detection algorithms. These benchmarks aim to replicate key structural and dynamic properties of real-world networks, providing controlled environments for testing. However, given the diversity of network types and behaviors, no single benchmark can address all possible scenarios optimally [51]. Established benchmarks often incorporate small-world properties [62] and scale-free characteristics [3], using network growth and preferential attachment to maintain power-law degree distributions. However, some of the most widely used benchmark networks are based on the planted l -partition model [11], such as the Girvan–Newman model [18], where inter- and intra-community link probabilities are predefined, leading to the formation of distinct clusters. These models, however, often result in networks with homogeneous degree distributions, which do not accurately reflect the complexity of real-world networks. To address this, the LFR benchmark was introduced [35], incorporating power-law distributions for node degrees and community sizes, as well as a mixing parameter to control the proportion of edges that connect different communities. This approach provides a more realistic representation of the structural diversity observed in real-world networks. Extensions to the LFR benchmark [34] accommodate more complex scenarios, including directed, weighted, and overlapping communities, and have been adapted to dynamic networks (see, e.g., [36, 21]). However, these dynamic adaptations can lead to unpredictable community evolution due to the influence of random processes. To this end, Aldecoa [1] introduced a “closed” benchmark with predefined initial and final states, where links are rewired gradually to ensure controlled transitions.

Over the last decade, many more temporal network benchmarks have been developed. Notable examples include Granell et al. [20], who proposed cyclic networks based on SMB models to simulate events like community splits, merges, growth, and shrinkage, combining these into mixed benchmarks. Rossetti [53] introduced RDyn, where intra-community relations evolve based on probabilities, with stability measures triggering community events. Bazzi et al. [5] used probabilistic rules for copying community memberships between snapshots, adding edges via a degree-corrected SBM. Cazabet et al. [9] employed event instructions (e.g., split, merge, birth, death) to govern community evolution, rewiring edges with the Deterministic Strongly Assortative Block Model (DSABM). Lastly, Longa et al. [37] created synthetic surrogate networks mimicking complex system dynamics.

All of these benchmarks aim to replicate the properties observed in real-world dynamical systems as closely as possible. However, accurately modeling all relevant features of such systems becomes increasingly challenging, especially when the systems exhibit significant noise or highly stochastic behavior. This complexity often requires a careful balance between incorporating realistic dynamics and maintaining computational feasibility. Selecting an appropriate benchmark requires careful consideration to ensure it aligns well with the specific characteristics of the system under study, along with proper tuning of parameters to achieve meaningful results.

3.2 A New Agent-Based Network Generator

In this subsection, we introduce a new agent-based temporal network generator designed to address the challenges outlined earlier. Our main idea for obtaining network snapshots is to simulate the dynamics of N agents (also called particles) in a two-dimensional space, governed by the diffusion process

$$dX_i(t) = -\nabla U_i(X_i(t)) dt + \sqrt{2\beta^{-1}} dW_i(t),$$

where $X_i(t)$ is position of the i th agent at time t , β determines noise intensity, U_t is a time-dependent potential, and $W_i(t)$ is a standard Brownian motion [15]. At each time step, agents represent nodes of a static network, i.e., a snapshot of a temporal network, with edges formed probabilistically based on spatial proximity: the closer two agents are, the higher the probability of an edge between them. In this way, we can synthesize both unweighted and weighted network snapshots. To impose metastability on the benchmark network, we use a time-evolving potential U_t with discrete changes over the simulation time, creating intervals where agents settle near potential minima, forming stable configurations or phases. The shape of U_t leads to the emergence of densely populated regions, resulting in community formation in the network. Changes in the potential perturb the dynamics, leading to the reorganization of agents within the simulation space, which characterizes a shift between two phases. Additional details on the generator’s design and implementation can be found in Appendix A.

3.3 Performance Analysis on Synthetic Examples

To validate the performance and robustness of our proposed LNE and IMC methods (introduced in Section 2), we conduct experiments on both synthetic and real-world datasets. The following two sub-sections focus on an evaluation based on two synthetic datasets generated using our agent-based temporal network generator. They are designed to highlight different aspects of community dynamics, such as the presence and intensity of noise, density of connections, and the nature of community evolution. In Section 4, we will evaluate our method using real world datasets. A short summary of all used datasets is given in Table 1.

The experiments will be carried out using a range of different exploration times τ across examples to analyze their influence on detecting structural transitions. Additionally, accurate detection of these transitions relies on the proper choice of the bandwidth parameter σ for the Gaussian kernel. We choose σ in all experiments using grid-search to optimize for the kernel’s ability to distinguish between similar snapshots (within the same phase) and dissimilar ones (across different phases). Specifically, we choose σ such that it maximizes the variance within the entries of the Gram matrix K , enhancing its discriminative power. Following this approach, in the LNE experiments on the synthetic data, the Gaussian kernel is chosen with bandwidth parameter $\sigma = 0.5$. A summary of all parameters used in the LNE and IMC algorithms across all examples is provided in Table 2. The following subsections present descriptions and analyses of the two synthetic datasets, focusing on their properties and the insights gained from applying LNE and IMC to detect structural transitions and community dynamics.

3.4 Synthetic dataset 1: Community Split

The *Community Split* dataset is designed to illustrate a straightforward phase transition, where one community splits into two, as shown in Figure 6c. We will use this dataset to demonstrate how our methods handle noise and capture changes in community structure over time.

Dataset Properties: The dataset represents the movement of 120 agents over a total simulation time of $T = 7.5$, as shown in Figure 6c. The dataset comprises 15 snapshots, created by sampling the simulation every $r = 10$ steps starting from the 10th step. We use the potential function shown in Figure 6a that consists of two distinct configurations - or phases. Phase 1 spans snapshots 0-7 and phase 2 corresponds to snapshots 8-14. The parameters defining the potential are selected such that, in the first phase, two wells are present with a barrier separating them, and in the second phase, there are three wells. Snapshots of the agent dynamics can be seen in Figure 6c: in phase 1, the simulated agents form two communities localized around the minima of the wells. At the

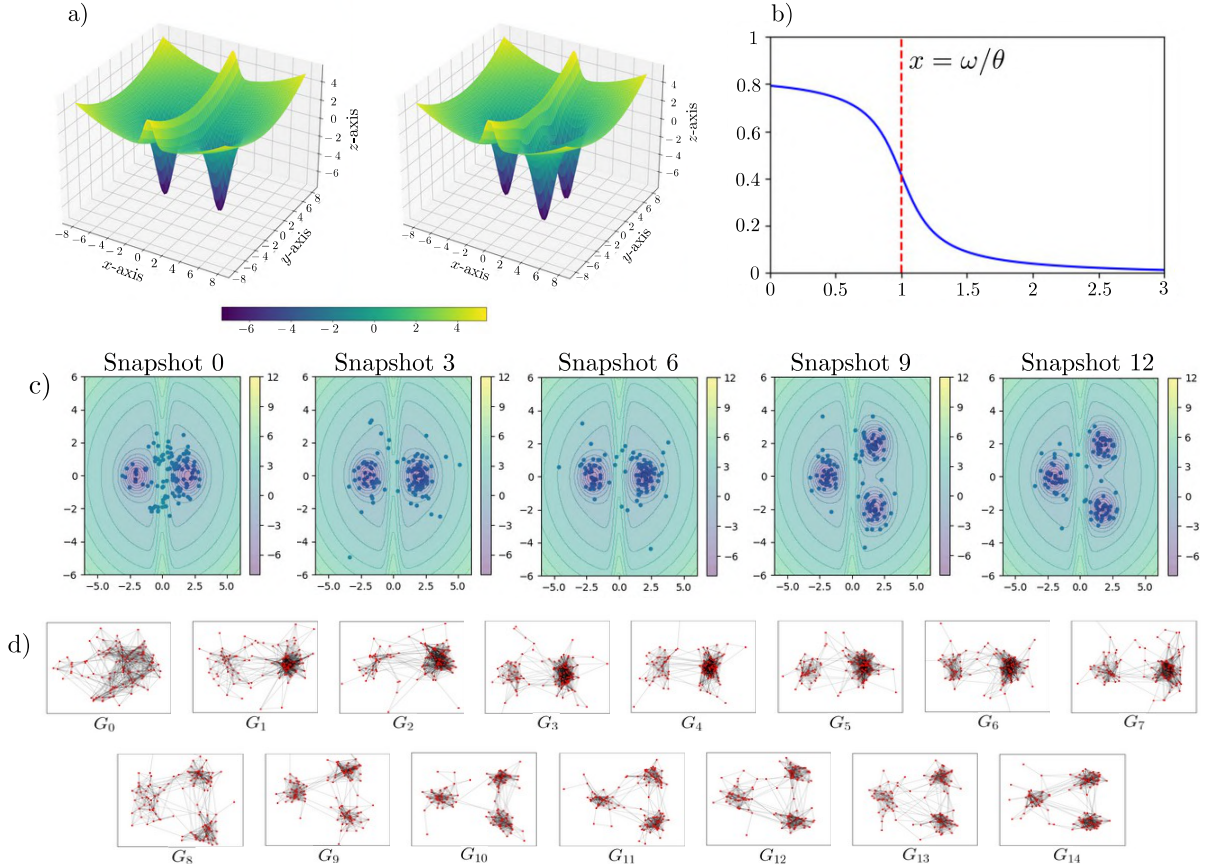


Figure 6: Construction of the *Community Split* dataset using our agent-based network generator. a) Potential function during two equally long periods of the total simulation time. b) Evaluation function for edge construction. c) Positions of the particles and the underlying potential across 5 snapshots. d) Full realization of a temporal network.

start of phase 2, the right well splits into two, causing the community of agents on the right to also split, inducing the phase transition. The resulting networks presented in Figure 6d are constructed based on agents' positions, such that an edge is created between two nodes if they are closer than a given threshold, with an edge weight defined by the evaluation function, shown in Figure 6b. The snapshots represent intervals of constant potential, ensuring consistent network structure within each phase. The noise intensity is set to $\beta = 0.45$, introducing relatively high variability in agent trajectories while preserving the overall community structure. The snapshots 0 to 7 correspond to Phase 1, and snapshots 8 to 14 represent Phase 2. This transition is initiated by the splitting of the right well, highlighting the generator's ability to simulate dynamic community evolution (see Figure 6d).

Results and Observations: Spectral analysis of the eigenvalues of the L_α generators reveals distinct spectral gaps that correspond to the number of communities in each phase. Specifically, in Phase 1, a gap appears after the second eigenvalue, indicating two communities, while in Phase 2, a gap emerges after the third eigenvalue, reflecting the presence of three communities. We illustrate this behavior in Figure 7a. Since all snapshots within a given phase share very similar community structure, their eigenvalues remain similar as well, and the spectral gap consistently appears at

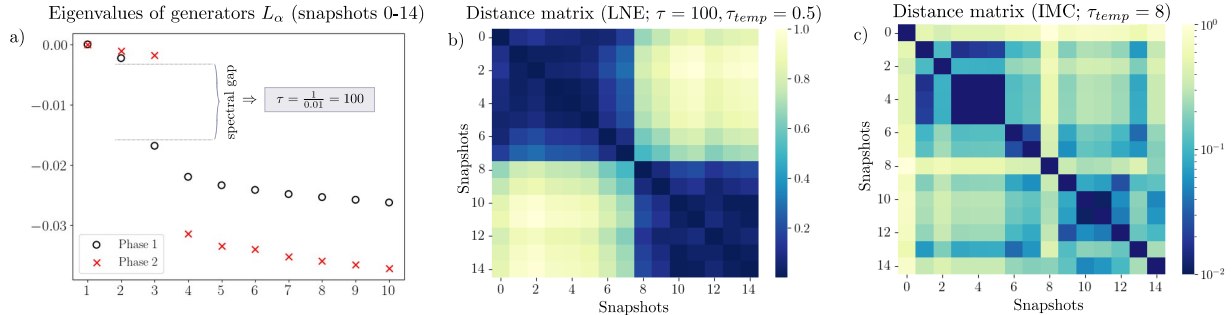


Figure 7: Results of LNE and IMC approaches on the Community Split dataset. a) Averaged eigenvalues of L_α across snapshots for both phases. Black circles correspond to snapshots 0-7, red crosses correspond to snapshots 8-14. b) Distance matrix obtained from LNE algorithm for $\tau = 100$ and $\tau_{temp} = 0.5$. c) Distance matrix obtained from IMC algorithm for $\tau_{temp} = 8$.

the same location. Therefore, instead of showing 10 largest eigenvalues for every generator L_α for $0 \leq \alpha \leq 14$, we show the average of each eigenvalue within Phase 1 ($0 \leq \alpha \leq 7$) and Phase 2 ($8 \leq \alpha \leq 14$). By doing so, we enhance visual clarity and highlight the general underlying community structure in the snapshots from both phases. Further analysis confirms that for exploration times τ in the range $1/0.015 \approx 67 \leq \tau \leq 200 = 1/0.005$, our method accurately identifies the community structure of both phases. In this example, we set $\tau = 100$. To group snapshots and further characterize phase transitions, we perform spectral clustering on the temporal transition matrix $P_{temp}^{0.5} = \exp(L_{temp}\tau_{temp})$, which corresponds to a continuous random process between the snapshots. The parameter $\tau_{temp} = 0.5$ was chosen based on the spectral gap observed in the spectrum of L_{temp} defined on the reduced network model. The resulting distance matrix (shown in Figure 7b) clearly shows the distinction between the two phases, with a sharp change between the 7th and 8th snapshot, corresponding to the splitting of the right community.

In comparison, the IMC method demonstrates lower precision in distinguishing the phases, which is a trade-off for its reduced computational costs. This is also reflected in the less distinct boundaries within the distance matrix. Nevertheless, some separation is still visible, with two diagonal blocks corresponding to the two phases. For IMC, we set $\sigma = 0.05$ and $\tau_{temp} = 8$. Table 3 provides a detailed comparison of the performance of LNE and IMC across all examples.

3.5 Synthetic dataset 2: Community Hierarchy

The second synthetic dataset, *Community Hierarchy*, is significantly larger than the Community Split dataset, characterized by denser connections within communities and reduced noise. This dataset is designed to demonstrate the hierarchical evolution of community structures across three distinct phases and highlight limitations of IMC. It exemplifies the generator’s ability to simulate complex community dynamics and showcases the method’s sensitivity to hierarchical changes, as well as its effectiveness in change-point detection at different resolutions.

Dataset Properties: The dataset consists of 210 snapshots representing the movement of 100 agents over a total simulation time of $T = 105$ with the step size $h = 0.05$, where snapshots are sampled every $r = 10$ steps. This dataset is divided into three phases of approximately equal duration. In Phase 1, the potential function contains two wells, one on the left and one on the right side of the simulation space, resulting in two communities. At $t = 32$ (snapshot $\alpha = 64$), the left well splits into two smaller wells, causing the left community to divide into two, marking the start of

Phase 2. At $t = 68$ (snapshot $\alpha = 136$), the right well similarly splits into two, initiating Phase 3. In this case, we set $\beta = 0.75$, reducing the noisy behavior of nodes compared to the Community Split example, and the edge evaluation function is defined with $\xi = 1, \nu = 0.9, \theta = 15, \omega = 22$. The resulting network is shown in Figure 8. Note that the communities on the left maintain closer spatial proximity, resulting in denser connections compared to the communities on the right. This creates a hierarchical structure, where the smaller communities on the left remain part of a larger overarching module.

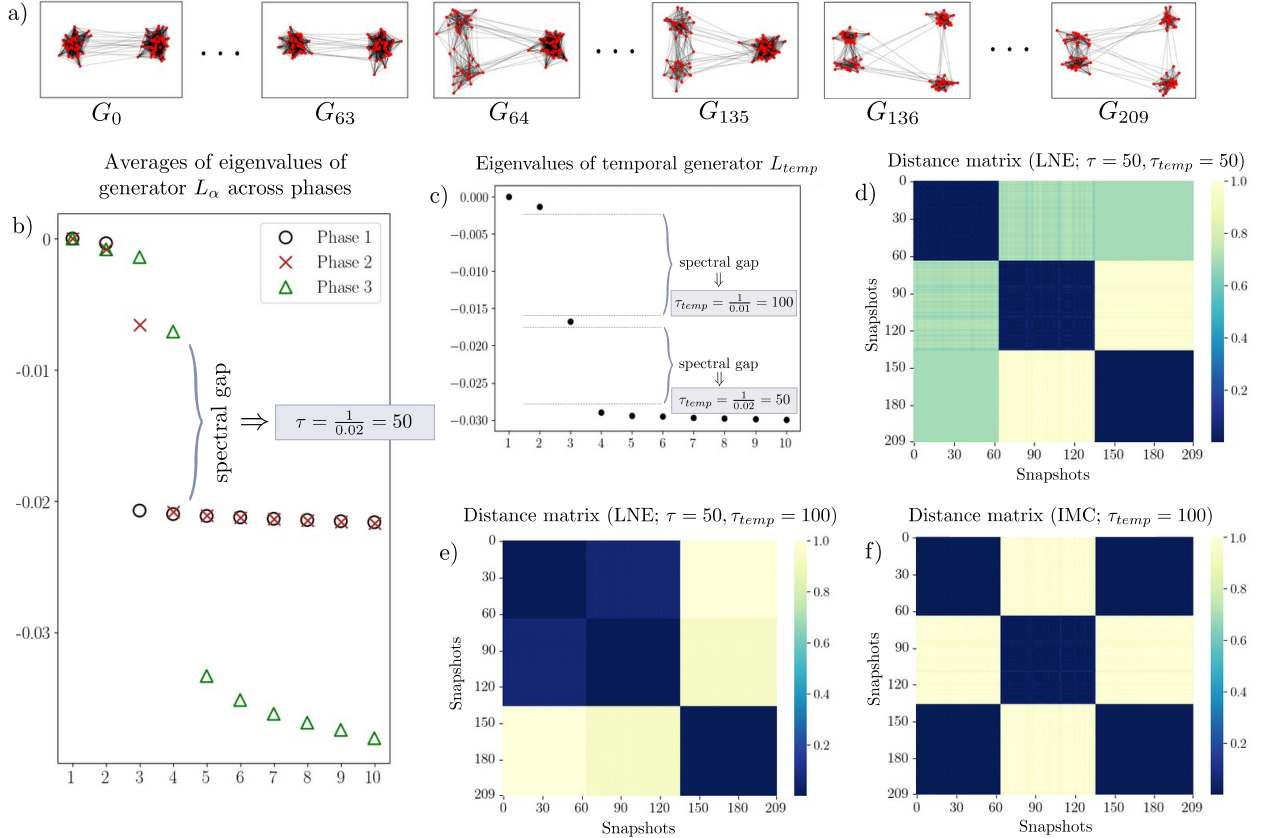


Figure 8: Results of LNE and IMC approaches on the Community Hierarchy dataset. a) Community Hierarchy dataset. b) Averaged eigenvalues of L_α across snapshots for all three phases. Black circles correspond to snapshots 0–63, red crosses correspond to snapshots 64–135 and green triangles correspond to snapshots 136–209. c) First ten eigenvalues of the temporal generator L_{temp} . d) Distance matrix for LNE, $\tau_{temp} = 50$. e) Distance matrix for LNE, $\tau_{temp} = 100$. f) IMC, $\tau_{temp} = 100$.

Results and Observations: Spectral analysis of the eigenvalues of the L_α generators shows clear spectral gap after 2nd, 3rd, and 4th eigenvalue for Phases 1, 2 and 3 respectively. Similarly to previous example, in Figure 8b averaged eigenvalues across snapshots for all three phases are shown together with the indicated spectral gap. Based on this analysis we choose $\tau = 1/0.02 = 50$. Further analysis of L_{temp} on the reduced network model reveals two possible spectral gaps in its eigenvalue spectrum (see Figure 8c). Using $\tau_{temp} = 100$ based on the first gap, our method detects two phases but does not distinguish the third due to the high interconnectivity of the left-side communities. Reducing τ_{temp} to 50, based on the second gap, successfully differentiates all three phases. The distance matrices between snapshots confirm these observations (Figures 8d, e). For $\tau_{temp} = 50$

three distinct blocks emerge, corresponding to the three phases. This means that the choice of the temporal exploration time determines the resolution level that is considered during phase clustering and change point detection. With lower τ_{temp} , localized, densely connected regions are treated as distinct modular structures, enabling a fine-grained analysis in the learning process. As the temporal exploration time increases, the walker has sufficient time to traverse somewhat less similar snapshots and algorithm becomes less sensitive to milder variations within communities that are part of larger modules. This flexibility allows for fine-tuning the algorithm’s sensitivity to the intensity of structural changes, offering an interesting balance between snapshots grouping into phases and change detection precision.

The IMC approach fails to detect the difference in the community structure between the first and the third phase, as illustrated in the distance matrix for $\sigma = 0.01$ and $\tau_{temp} = 100$ (Figure 8f). Specifically, all communities in both cases are of approximately the same size within snapshots, resulting in very similar invariant measures even though the number, size, and structure of communities is completely different between these two phases.

Having demonstrated the effectiveness of our method on synthetic datasets, we now turn our attention to more complex and real-world scenarios. In the following section, we apply our approach to real and simulated social dynamics data, showcasing its practical applicability across various domains of network analysis.

4 Experiments on Real-world Datasets and Social Dynamics Simulation Data

Having validated the robustness and flexibility of our methods on synthetic datasets, we now turn to their application in real-world scenarios. Real-world datasets often present unique challenges, such as incomplete data, noise, and complex, domain-specific dynamics. To demonstrate the practical utility of our approach, we apply it to diverse datasets spanning biological, sociological, and historical contexts. Specifically, we will use the following four datasets, which are also listed in Table 2: (1) Vibrio Cholerae Infection [26, 43] (real-world dataset of gut microbiota parameters of a Bangladeshi patient during the disease and recovery period), (2) Hunter-Gatherer interaction network [63] (underlying temporal network of the population dynamics of hunter-gatherer communities in Central Africa during the past 120 000 years), (3) Opinion Dynamics interaction network [23] (underlying network of the opinion dynamics of individuals in a social space affected by influencers and media presence), and (4) a protein-protein-interaction network during cell division [38] (temporal network modeling protein-protein interactions during the yeast cell division cycle). We should note that in Cholera and Hunter-Gatherer datasets we have several connected components or isolated nodes within snapshots. In such cases we treat each connected component independently and consider the probability distributions resulting from random walks on each component individually. The generator matrix L in this case has zero rows corresponding to isolated nodes. In these examples, we select τ as described in Section 2.6. Table 1 presents the averages of the expected waiting times at nodes across snapshots. The choice of τ is based on the ratio $\tau/(\text{avg. degree})$, which reflects the expected number of steps of a random walker during exploration phase. For datasets with dense community structure, such as the Opinion Dynamics dataset, a small ratio (1.44 in this case) is sufficient to capture the local structure effectively. In contrast, for datasets with sparser intra-community connections, such as the Cholera and Hunter-Gatherer datasets, a higher ratio (13.5 and 7.35, respectively) is selected to ensure adequate exploration of the community structure. The parameter σ is determined as described in Section 3.3, while τ_{temp} is directly computed from the spectral gap of L_{temp} . A list of the used parameters for all experiments is shown in Table 2.

Table 1: Summary of datasets used for the benchmark experiments

	#Nodes	Avg. #Edges/Edge weight	Avg. degree	#Snapshots	#Phases
Community Split	120	1137.2	18.95	15	2
Community Hierarchy	100	1551.3	31.03	210	2/3
Cholera	96	35.58	0.74	34	2
Hunter-Gatherer	393	2102.27	13.6	45	3
Opinion Dynamics	250	8666.83	69.34	167	2
Cell Division	83	135.65	3.26	102	2-11

4.1 Cholera Dataset

The first dataset that we will analyze originates from research conducted in Hsiao et al.[26] (see Melnyk et al.[43] for an analysis of this data). The focus of this study was to understand the changes in the gut microbiota during the course of *Vibrio cholerae* infection. The data was collected from a Bangladeshi patient over time, during different stages of the disease and convalescence period. Based on the total of 34 collected samples, a temporal network is constructed as described in Melnyk et al.[43] modeling the presence and correlations between operational taxonomic units (OTUs) during both disease manifestation and recovery phase. The average weighted degree of nodes in the OTU interaction network across the two phases is illustrated in Figure 9a. The results indicate the formation of different communities in each phase, corresponding to the patient’s health status. Our objective is to identify these two phases within the OTU data, as well as to detect the moment in time when the transition between infection and recovery period happened. Figure 9b shows the distance matrix obtained from LNE with $\tau = 10$, $\sigma = 2$, and $\tau_{temp} = 2$. The original study reports that the patient entered the recovery phase after snapshot 17, which closely aligns with the results of our method. The embeddings obtained from the second and third eigenvector of the temporal transition matrix are shown in Figure 9c, where data points are colored based on spectral clustering results. For the IMC experiments given in Table 3 we set $\sigma = 0.05$ and $\tau_{temp} = 10$.

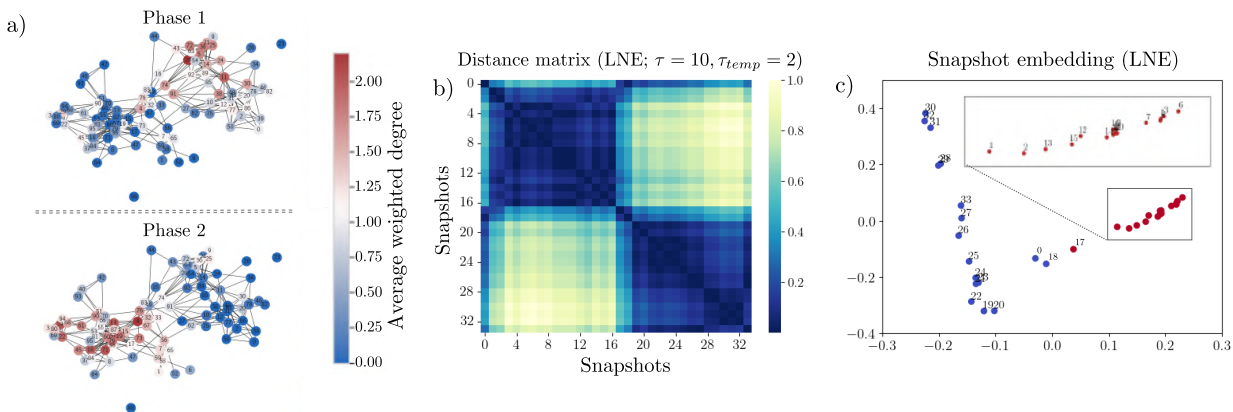


Figure 9: Results of the LNE approach applied to the Cholera dataset. a) Average weighted degree of nodes in the OTU interaction network across two distinct phases. b) LNE distance matrix for $\tau = 10$ and $\tau_{temp} = 2$. c) Snapshot embedding using the second and third eigenvector of the temporal transition matrix.

4.2 Hunter-Gatherer Dataset

In this example, we consider the Hunter-Gatherer dataset derived from simulations based on a model proposed by Zonker et al.[63]. The focus of this study was understanding the impact of environmental shifts, social structures, and demographic factors on the emergence and dispersion of cultural traits throughout human history. The research has been conducted using empirical and reconstructed data from Central Africa spanning 120 000 years, and an agent-based model was developed for the simulation of hunter-gatherer populations, their demographic dynamics, mobility patterns, and cultural interactions. The authors validated their findings against real-world data obtained from hunter-gatherer populations in Central Africa. Hunter-gatherer camps are represented as agents that adapt their positions in the space based on a suitability landscape function. This function depends on bio-climatic conditions of the geographical region and is constructed using the environmental niche model [49]. During the simulation, agents gravitate towards regions with favorable living conditions. Networks are formed based on a predefined interaction radius, which is set to 10 in our case. The suitability landscape changes every 15 time steps and these intervals serve as ground truth for the metastable states of the system. In our experiment, we consider a segment of the hunter-gatherer temporal network consisting of 45 consecutive snapshots and three different suitability landscape functions. The model simulation is conducted using the code the original publications[64, 63]. Snapshots presented in Figure 10a illustrate the suitability landscape across three phases showing the population distribution at 117 827 years before present (BP), 114 575 BP and 113 121 BP. In the first phase, agents form many small communities across the simulation region. As the suitability landscape evolves, the majority of agents concentrate in two densely connected areas: one along the west coast and the other inland. Eventually, the inland suitability minimum fragments into several smaller minima, leading to a redistribution of agents across these newly formed valleys. In this dataset, we set $\sigma = 2$ in kernel evaluations. In Figure 10b, we show the distance matrix for LNE for $\tau = 100$ and $\tau_{temp} = 0.5$ and the embedding space with clustered snapshots, that clearly shows separation into the three phases matching the suitability landscape changes. In IMC experiments we set $\sigma = 0.02$ and $\tau_{temp} = 4$.

4.3 Opinion Dynamics Dataset

In recent years, the field of social dynamics has received substantial attention for its efforts to model the movement of individuals in the social space and investigate their interaction and the subsequent evolution of opinions. Individuals can have various roles in the social space and possess the ability to strongly influence the beliefs of other people and, to a certain extent, also the dynamics of the entire social system. The permanent pillars around which individuals tend to construct their opinions are represented by traditional media, integrated within social platforms. Conversely, influencers, who are private individuals with a significant number of followers, enter and exit the social media space at a significantly faster rate, generate content on trending topics, and modify their behavior and opinions to attract the maximum number of followers. Although they are able to attract audiences at a faster pace than traditional media, their capacity to retain followers in the long term is relatively restricted[23].

In this example, we consider an agent-based model of social dynamics based on Helfmann et al.[23, 24]. This simulation models the opinions of $N = 250$ individuals in a 2-dimensional opinion space $D \subset \mathbb{R}^2$ with $L = 4$ influencers and $M = 2$ traditional media agents. In our simulation, individuals initially adopt opinions uniformly from the set $\{(x, y) | x \in [-7, -4] \cup [4, 7], y \in [-2, -0.5] \cup [0.5, 2]\}$ consisting of four disjoint regions. Each individual within a region subscribes to the designated influencer and each influencer adopts the average opinion of their respective

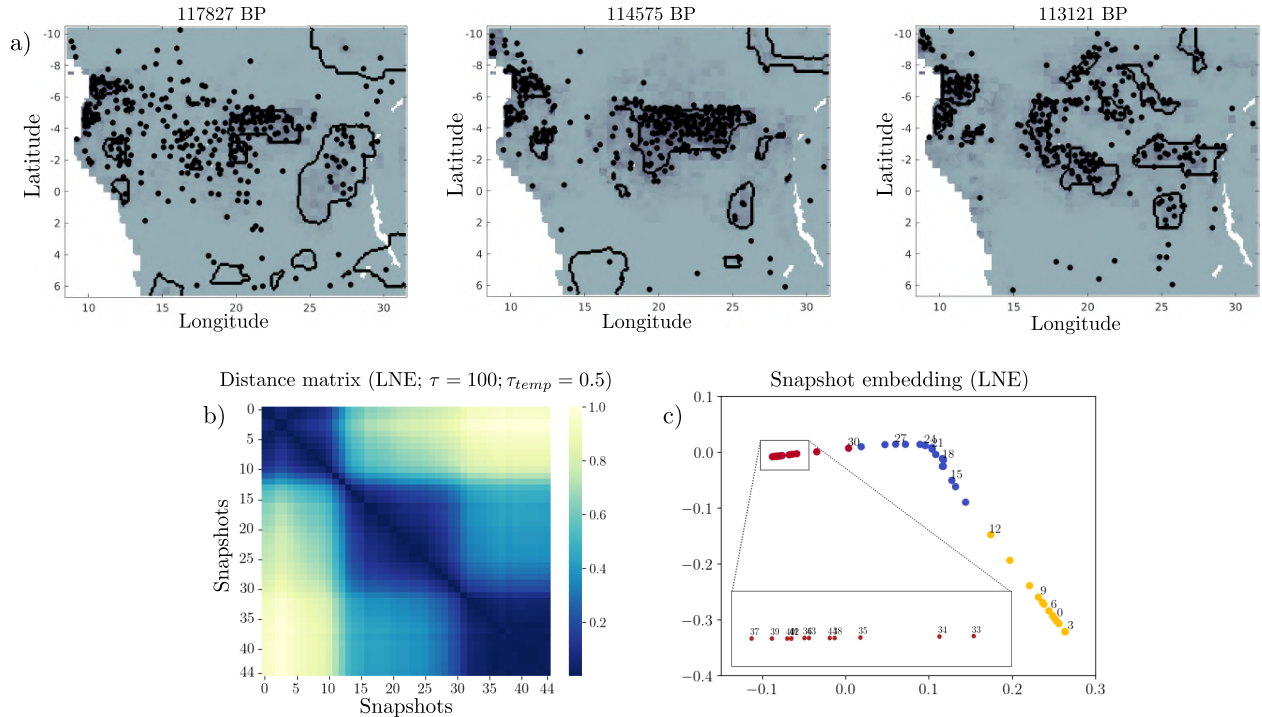


Figure 10: Results of the LNE approach applied to the Hunter-Gatherer dataset. a) The first three suitability landscapes of the Hunter-Gatherer dataset along with the agent distribution at times 117827 BP, 114575 BP and 113121 BP. b) LNE distance matrix for $\tau = 100$ and $\tau_{temp} = 0.5$. c) Clustered embeddings of the Hunter-Gatherer dataset.

followers. Positioned initially at $(0, -1.5)$ and $(0, 1.5)$ media agents are followed by individuals positioned on the corresponding side of the x -axis. During the simulation, individuals interact with each other based on the underlying relational network (in this example the relational network is complete) and each of them follows exactly one influencer and one medium. The opinion dynamics of individuals is governed by a stochastic differential equation, which includes interaction forces from other individuals, media, and influencers. Influencers adjust their opinions based on the average opinion of their followers, while media agents update their opinions at a slower rate (see Helfmann et al.[23] for details and default parameter values). The simulation is conducted over 5000 iterations where snapshots are taken with a step size of 30 iterations. A weighted temporal network is then constructed over the set of individuals, where the edge weights at each snapshot are given with $w_{ij}(t) = \exp(-|x_j(t) - x_i(t)|)$ where $x_i(t)$ represents the opinion of individual i at time t (following the original approach).

After applying LNE to this temporal network, we recover two phases of the system as shown in the distance matrix in Figure 11c. The first phase corresponds to the period preceding the merging of communities, while the second one to the period when all individuals belong to one of the two distinct communities. Since the silhouette score assesses the quality of clustering individuals within each snapshot, we use it to identify the ground truth phases of this dataset. The transition point between the phases with 4 and 2 communities is defined as the first snapshot where the average silhouette score, computed over 5 iterations for 2-clustering, exceeds that for 4-clustering. All clusterings of individuals are performed using k -means. A visual representation of four snapshots showing the current positions of agents across various time points is given in Figure 11a. The black circle and triangle represent two media sources, influencers are illustrated as colored circles, and

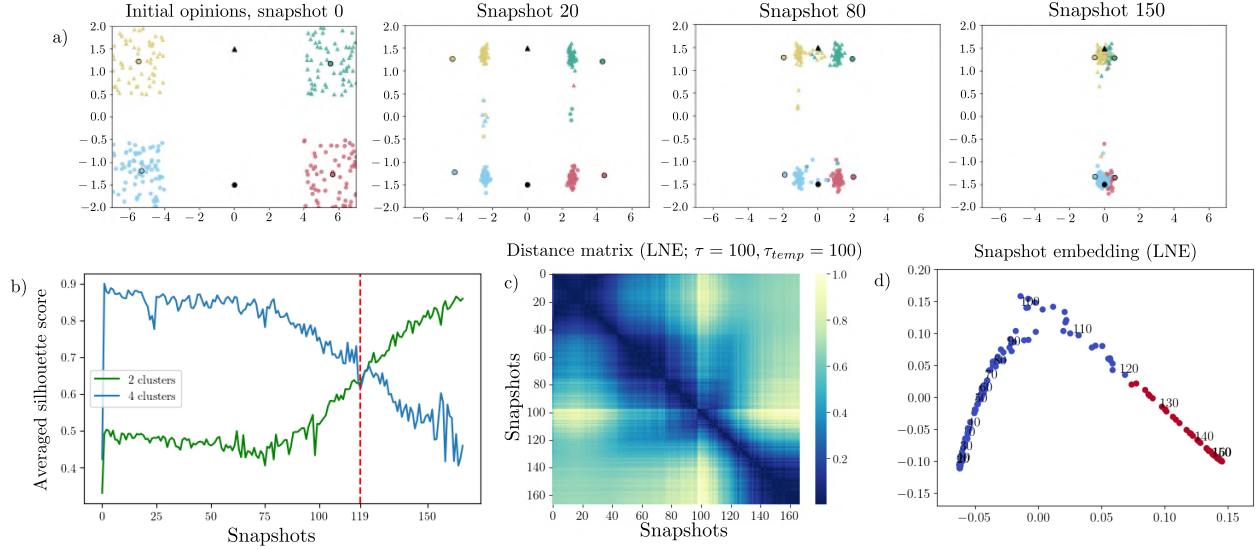


Figure 11: Results of the LNE approach applied to the Opinion Dynamics dataset. a) Initial positions of agents. Individuals grouped around 4 influencers gravitate towards 2 media outlets, ultimately forming only 2 distinct communities. b) Averaged silhouette scores over 5 iterations for 2- and 4-clusterings. c) LNE distance matrix for $\tau = 100$ and $\tau_{temp} = 100$. d) Clustered embeddings of the Opinion Dynamics dataset.

individuals take on the shape of the media they follow and adopt the color of the influencer they are subscribed to. Initially, individuals are randomly distributed within designated regions of the opinion space. Influencers adopt the average opinion of their followers, so the individuals form four communities in the vicinity of the corresponding influencer. They gradually gravitate towards the media outlet they follow, until the communities in the upper and lower half-planes of the social space start to merge. Ultimately, individuals are divided into two discernible communities. In this dataset we set $\tau = 100$, $\sigma = 1$ and $\tau_{temp} = 100$ in LNE. As mentioned in Section 2.4, the IMC algorithm encounters difficulties in distinguishing between phases due to the similar sizes of communities within all snapshots. Hence, the ARI value remains at 0 regardless of parameter selection. For this experiment, we set $\sigma = 0.01$ and $\tau = 13$. This example is of particular interest because all the snapshots are complete networks with different interaction strength (weights) between the nodes. As shown in Table 3 most of the methods had difficulties in handling this gradual transition period and detecting a clear change point. Our approach and GraphKKE managed to obtain a decent ARI value. Note that GraphKKE works only with unweighted networks (see Remark 5.1). Thus, in this case, we adapt the dataset by introducing an edge cut-off threshold to get the best outcome (see Section 5.2 for details).

4.4 Cell Division Dataset

As a last example, we consider a biological real-world dataset from a study by Lucas et al. [38] on yeast cell division cycles. Simply put, cells undergo four main biological phases before dividing into two: first cells grow to the necessary size in the first phase (G1), followed by DNA synthesis (S phase), a second gap phase (G2), and finally mitosis (M phase), where duplicated chromosomes are evenly divided into two daughter cells. Cell division is regulated through the interactions between proteins, which can be modeled as a protein-protein interaction (PPI) network [38, 47]. In PPI networks, nodes represent proteins, whereas the weighted edges represent the interactions among

them. To model the temporal network of protein interactions during the yeast cell cycle, data from the static PPI network are enhanced with temporal series data on edge activity. This enhancement involves numerical derivations of protein concentrations over time, based on an existing ODE model that describes the interactions for approximately 21% of the proteins [10]. The granularity of the time snapshots of the network is dictated by the time step intervals used in the ODE’s numerical integration. Evolving edge weights are calculated using available data, representing the simultaneous presence of corresponding proteins at specific times (and are subsequently normalized). Lastly, weights for the remaining edges from the static PPI network are uniformly assigned a value of 1. Due to the changes in protein-protein interactions following transitions between different phases of a cell cycle, the structure of network snapshots should exhibit consistency within the same phase, while significant changes in the network structure are expected to occur following a phase transition. The authors developed the *Phasik* algorithm that allows to detect k groups of structurally similar snapshots for a predefined parameter k . They obtained 10 partitions of the network for k ranging from 2 to 11. Although this dataset is not expected to exhibit pronounced community structures, we apply our LNE and IMC algorithms here as well and compare the results with clusterings from the original paper[38] to test their performance in a more generalized setting (Figure 12). In this experiment we set $\tau = 10, \sigma = 0.6, \tau_{temp} = 50$ in LNE and $\sigma = 0.01$ and $\tau_{temp} = 50$ in IMC. The results demonstrate that the phases we detected align closely with those reported by the original authors, particularly for smaller values of k . One exception is the case of $k = 2$, where our method isolated only the S phase from the others, whereas the original algorithm grouped the G1 and S phases together, separating them from the G2 and M phases. Additionally, we observe that the transition between the G2 and M phases occurs later in the network’s evolution across all k . This phenomenon, also noted in the original results, is attributed to a sharp change in edge weights between specific protein interactions. Biologically, this corresponds to the metaphase checkpoint, where chromosomes are expected to achieve proper bipolar attachment to the mitotic spindle.

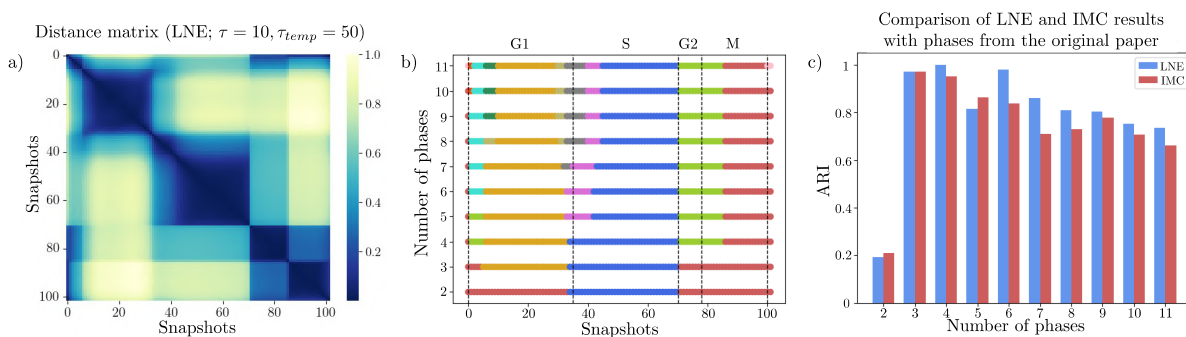


Figure 12: Results of LNE and IMC performance on the Cell Division dataset. a) LNE distance matrix for $\tau = 10$ and $\tau_{temp} = 50$. b) Phases inferred for k ranging from 2 to 11. c) Comparison of LNE and IMC results with the clusterings from the original paper.

5 Benchmarking Community Detection in Temporal Networks: A Comparative Review

As discussed above, analyzing community dynamics in temporal networks presents unique challenges. Methods are required that can accurately detect structural transitions while maintaining computational efficiency. The growing interest in this area has led to the development of diverse approaches,

Table 2: Parameter values for our LNE and IMC methods, used in the benchmark experiments

	LNE			IMC	
	τ	σ	τ_{temp}	σ	τ_{temp}
Community Split	100	0.5	0.5	0.05	8
Community Hierarchy (2 phases)	50	0.5	100	0.01	100
Community Hierarchy (3 phases)	50	0.5	50	0.01	100
Cholera	10	2	2	0.05	10
Hunter-Gatherer	100	2	0.5	0.02	4
Opinion Dynamics	100	1	100	0.01	13
Cell Division	10	0.6	50	0.01	50

ranging from spectral clustering to machine learning-based embeddings. To provide the reader with a clearer understanding of the field, we first summarize some of the existing key methods and then present a comparative analysis of these methods with our methods.

5.1 Methods for Community Detection in Temporal Networks

Numerous algorithms have been developed for community detection in static and temporal networks. While static methods like modularity optimization [46] and spectral clustering [61] are well-established, their extensions to temporal networks face challenges due to the dynamic nature of evolving communities [27]. Approaches tailored to temporal networks often aim to identify structural similarities across time points and to detect significant changes, such as community splits/merges, births/deaths, or complete reorganizations. For instance, Peel et al.[50] utilize probabilistic models like generalized hierarchical random graphs to find change points, while transfer operator methods [43, 31] leverage spectral properties of stochastic processes to capture transitions.

A key direction in temporal network analysis is the development of methods that learn low-dimensional embeddings of network snapshots, capturing their structural information and enabling the detection of (meta-)stable states and transitions in this new feature space. While much of the existing work focuses on embedding nodes or edges in static networks [52, 22, 17], fewer approaches address the challenge of embedding entire snapshots for temporal networks [25, 39] or even temporal networks as a whole [12]. This remains an active area of research, with significant potential for applications in analyzing evolving systems. Next, we outline several key methods that aim to derive low-dimensional representations of snapshots and discuss their comparative performance in Section 5.2.

Principal Component Analysis (PCA). PCA is a standard dimensionality reduction algorithm that discovers new uncorrelated variables, also called principal components, in large, high-dimensional datasets such that only a first few of them contain as much information as possible about the system. In other words, it creates a new coordinate system such that most variance in the data is aligned with the direction of the first principal component. Each subsequent component captures the maximum remaining variance while being orthogonal to the previous components. We will apply PCA on the set of time-snapshots adjacency matrices.

Graph Kernel Koopman Embedding (GraphKKE) employs transfer operators to detect structural changes in temporal networks [43]. These operators, such as adjoint Perron–Frobenius and Koopman operators, describe the evolution of probability densities and observables in stochastic processes. While these operators are infinite-dimensional, their spectral properties can be approximated using,

e.g., kernel methods. For temporal networks, snapshot similarities are captured using kernel evaluations between snapshots and their time-lagged versions. The resulting spectral gap in the eigendecomposition reveals the number of metastable states, with eigenfunctions providing low-dimensional embeddings of the snapshots.

Transformer + Contrastive Learning. (T+CL) is an unsupervised transformer-based approach [44]. Each snapshot is represented by a “master node”, connected to all other nodes and assigned a learnable vector. The method employs extended adjacency matrices as masks in multi-head attention layers to capture the topological structure of the snapshots. The algorithm computes node embeddings, where master node embeddings serve as low-dimensional representations of the entire snapshots. Additionally, the method considers the temporal order of snapshots by using the embeddings of several preceding snapshots as part of the input information while learning the next representation. Contrastive learning is then applied to group structurally similar snapshots closely in the embedding space while separating those from different phases, using the InfoNCE [60] loss function.

tdGraphEmbed integrates temporal information to create low-dimensional representations of entire snapshots [7]. This approach uses an unsupervised natural language processing (NLP) technique with a *word2vec* based architecture [45]. The algorithm utilizes information collected via random walks implemented as in Grover et al.[22] that incorporate tunable hyperparameters p and q to regulate the BFS and DFS biases of the walks. These walks collectively form a document that encodes the network’s snapshot at that specific time. Additionally, a learnable vector representing the entire snapshot G_α is given, and the goal is to maximize the likelihood of observing G_α given the corresponding document. This extends the CBOW model to encode both node relationships and snapshot-level features.

Together, these methods demonstrate a range of techniques for analyzing temporal networks by embedding snapshots in low-dimensional spaces. Their comparative evaluation, discussed in the next section, provides insights into how these approaches perform across synthetic and real-world datasets.

5.2 Comparative Analysis

In this section, we will compare the performance of our LNE and IMC approaches to the algorithms described in the previous section, showing their performance on the introduced synthetic and real-world datasets. We set the following method specific parameters. In all examples, we set the number of components in PCA to 2. In GraphKKE, we set the number of iterations $h = 1$, regularization parameter $\eta = 0.1$ and lag time $\tau = 1$. Since GraphKKE accepts only unweighted networks (see Remark 5.1), where edges can only have weights 0 or 1, we used grid search to identify the best edge cut-off parameter. Accordingly, we preprocessed the Opinion Dynamics dataset by removing all edges with weights below 0.15, and assigning a weight of 1 to the remaining edges. In the Cholera dataset as in the original paper all edges with positive weight are kept and assigned a new weight equal to 1. In T+CL we set batch sizes to 15 for Community Split, 64 for Community Hierarchy and Opinion Dynamics, 6 for Cholera and 16 for Hunter-Gatherer. The rest of parameters are set at default values as in Melnyk et al.[44] In *tdGraphEmbed* we set $p = 1$ and $q = 6$ so that random walks used for representation learning to explore their originating communities. The number of walks simulated from each node of each snapshot is set to 40 and their length to 50. The learning process is carried over 50 iterations and the dimension of the embedding space is 128. To allow the *tdGraphEmbed* algorithm time to learn, several initial embeddings are excluded from the ARI computation.

The following publications and codes were used to check and test the performance of the methods

described in Section 5 on our datasets:

1. *Principal Component Analysis (PCA)*: PCA module of the `scikit-learn` library.
2. *Graph Kernel Koopman Embedding (GraphKKE)*: [43] and the code from GitHub repository [41].
3. *Transformer + Contrastive Learning (T+CL)*: [44] and the code from GitHub repository [42].
4. *tdGraphEmbed*: [7] and the code from GitHub repository [6].

Remark 5.1 *The GraphKKE algorithm approximates transfer operators using kernel evaluations applied to snapshot adjacency matrices. However, this approach is not always suitable for comparing community structures across snapshots (see Remark 2.1). Even though in our work we use Gaussian kernel and the GraphKKE implementation by Melnyk et al. [43] incorporates both Gaussian and Weisfeiler-Lehman kernels, we chose to focus on the latter implementation for our experiments. This decision was guided by the authors’ findings, which reported superior performance of the Weisfeiler-Lehman kernel over the Gaussian kernel.*

Table 3: Adjusted rand indices (ARI) between ground truth and snapshot clustering using different methods. An ARI of 1 indicates perfect agreement with the ground truth, while 0 indicates completely different results. Numbers in bold indicate the best result for each dataset.

Dataset	LNE (ours)	IMC (ours)	PCA	GraphKKE	T+CL	tdGraphEmbed
Community Split	1	0.5	0.76	0.03	1	0
Community Hierarchy (2 phases)	1	0.14	0.94	0.18	0.8	0.24
Community Hierarchy (3 phases)	1	0.66	1	0.39	0.84	0.32
Cholera	0.88	0.77	0.77	0.88	0.74	0.05
Hunter-Gatherer	0.93	0.74	0.25	0.45	0.38	0.44
Opinion Dynamics	0.87	0	0	0.88	0	0.32

The results from the comparative analysis as outlined in Table 3 emphasize the strengths and limitations of the evaluated methods, particularly the robustness and flexibility of LNE in detecting community transitions across diverse datasets. While LNE demonstrated superior performance, its computational demands and areas for potential enhancement invite further investigation. In the following section, we reflect on these insights, discussing the broader implications of our results and outlining directions for future work to address the remaining challenges.

6 Discussion & Outlook

The results presented for the synthetic and real-world datasets highlight the robustness of the proposed Local Neighborhood Exploration (LNE) and Invariant Measure Comparison (IMC) methods. LNE demonstrated superior performance in detecting community transitions and identifying metastable phases, particularly in scenarios with complex dynamics, such as hierarchical structures or gradual transitions. IMC on the other hand, while computationally more efficient, was less effective in capturing subtle changes in more complex scenarios. The comparative analysis revealed that existing methods often require significant preprocessing or struggle with weighted networks, limiting their applicability. In contrast, LNE effectively uncovered transitions and stable phases in challenging datasets, such as the Cholera and Opinion Dynamics examples, showcasing its ability to provide

actionable insights for real-world systems, coming from diverse domains such as biology or the social sciences.

Although LNE offers high accuracy, there is still room for improvement in optimizing the algorithm’s performance. Future work could explore optimization techniques, such as sparse matrix representations or adaptive exploration times, to improve scalability. Additionally, we plan to extend the method to fuzzy clustering of time snapshots, where snapshots are not rigorously attributed to a certain phase. Instead, they could be assigned to a certain phase with a membership value, which would allow for more flexibility when analyzing the network structure and detecting change points. This approach could also help us to identify transition periods between phases, such as merging or splitting, during which snapshots are not assigned to any single phase. Moreover, as illustrated in the guiding example, not all nodes have to be members of communities (*member nodes*). Random processes originating from nodes not belonging to any community (*free nodes*) will gravitate toward their closest community since they move quickly through simple regions of the network. It is important to note that our snapshot encoding approach may not yield satisfactory results when the internal structure of communities remains stable, but a drastic reorganization among free nodes occurs. However, this can potentially be mitigated by initially detecting the member nodes and extracting the strength of connections between communities from the rest of the network. Our method can then be applied to this reduced dataset, focusing on tracking disruptions within communities. In Sections 3 and 4, we considered examples where all nodes are member nodes, while mixed scenarios involving both free and member nodes will be explored in greater detail in future work. Finally, we plan to further reduce the computational complexity of the algorithm. That is, random processes starting within the same community behave similarly in the long term. This suggests that the most valuable information about the network’s community structure is contained within the main transition pathways between communities. By these means, we can extract crucial information about how communities are organized within snapshots, filtering out less important details, and significantly simplifying the data under consideration. We expect that these improvements will enhance the scalability and overall performance of the method, making it even more effective for handling complex applications.

7 Conclusion

In this paper, we introduced a novel method for temporal network analysis based on random walk processes, which effectively captures community structure changes in temporal networks. The method identifies periods of network stability (network phases) and detects significant structural changes, such as splits, merges, or the formation and dissolution of communities. To this end, the proposed approach makes use of random walk processes on spatial and temporal scales to first learn the community structure of snapshots and then partition them into phases of structural stability. The method also learns low-dimensional vector representations of snapshots such that they preserve similarities in community structure and reflect each snapshot’s phase affiliation within the embedding space. Furthermore, we proposed a new, highly customizable benchmark network generator for testing the efficacy of our algorithm. We further validated our method on various synthetic and real-world datasets and demonstrated that it performs better than several existing state-of-the-art algorithms. These experiments underscored its versatility and robustness across a range of applications, from social dynamics to biological systems. Therefore, our method provides a powerful tool for analyzing complex, temporal networks and gives valuable insights into the dynamics of large-scale systems.

Our approach shows promising results on various synthetic and real-world datasets. Notably,

our method achieves better computational efficiency compared to most existing approaches in this domain, which typically scale at least quadratically with the number of nodes. This makes our approach well-suited for large-scale temporal network analysis. Future work will aim to further enhance scalability by investigating optimizations such as leveraging sparse matrix representations and employing adaptive exploration times to reduce computational complexity while preserving accuracy. At the same time, our method learns low-dimensional representations of entire snapshots of temporal networks, a capability for which only a limited number of techniques exist in the current literature, as discussed in Section 5.1. Furthermore, our method outperforms state-of-the-art representation learning methods in both community structure and phase detection accuracy. The robustness is also evident in networks with a gradual transition between phases, where other methods often struggle.

Data availability

The synthetic data generated in this work is available from the authors upon request. All real-world datasets used in this paper are publicly available (see [41, 64, 24, 32]).

Code availability

The code developed in this work is available from the authors upon request.

Author contributions

T.C., N.D.C. and S.K. were involved in planning and supervised the work. F.B. and N.D.C. developed the theoretical foundation of the method. F.B. implemented the method and performed the numerical simulations and experiments. All authors discussed the results and contributed to the final manuscript.

Funding

This work was supported by the German Ministry for Education and Research (BMBF) within the Berlin Institute for the Foundations of Learning and Data—BIFOLD (project grants 01IS18025A and 01IS18037I) and the Forschungscampus MODAL (project grant 3FO18501) and by the Deutsche Forschungsgemeinschaft (DFG, German Research Foundation) under Germany’s Excellence Strategy via MATH+: The Berlin Mathematics Research Center (EXC-2046/1, project ID: 390685689).

Competing interests

The authors declare no competing interests.

References

- [1] R. Aldecoa and I. Marin. Closed benchmarks for network community structure characterization. *Physical review. E, Statistical, nonlinear, and soft matter physics*, 85:026109, 02 2012.

- [2] P. Bajardi, A. Barrat, F. Natale, L. Savini, and V. Colizza. Dynamical patterns of cattle trade movements. *PLOS ONE*, 6(5):e19869, 2011.
- [3] A.-L. Barabási and R. Albert. Emergence of scaling in random networks. *Science*, 286(5439):509–512, 1999.
- [4] D. S. Bassett, N. F. Wymbs, M. A. Porter, P. J. Mucha, J. M. Carlson, and S. T. Grafton. Dynamic reconfiguration of human brain networks during learning. *Proceedings of the National Academy of Sciences*, 108(18):7641–7646, 2011.
- [5] M. Bazzi, L. G. S. Jeub, A. Arenas, S. D. Howison, and M. A. Porter. A framework for the construction of generative models for mesoscale structure in multilayer networks. *Phys. Rev. Res.*, 2:023100, Apr 2020.
- [6] M. Beladev. tdGraphEmbed: Temporal dynamic graph-level embedding. <https://github.com/moranbel/tdGraphEmbed>, 2020. Accessed: 2024-08-02.
- [7] M. Beladev, L. Rokach, G. Katz, I. Guy, and K. Radinsky. tdgraphembed: Temporal dynamic graph-level embedding. In *Proceedings of the 29th ACM International Conference on Information & Knowledge Management, CIKM '20*, page 55–64, New York, NY, USA, 2020. Association for Computing Machinery.
- [8] S. Boccaletti, V. Latora, Y. Moreno, M. Chavez, and D.-U. Hwang. Complex networks: Structure and dynamics. *Physics Reports*, 424(4):175–308, 2006.
- [9] R. Cazabet, S. Boudebza, and G. Rossetti. Evaluating community detection algorithms for progressively evolving graphs. *Journal of Complex Networks*, 8(6):cnaa027, 03 2021.
- [10] K. Chen, A. Csikász-Nagy, B. Györfy, J. Val, B. Novak, and J. Tyson. Kinetic analysis of a molecular model of the budding yeast cell cycle. *Molecular biology of the cell*, 11:369–91, 02 2000.
- [11] A. Condon and R. M. Karp. Algorithms for graph partitioning on the planted partition model. *Random Structures & Algorithms*, 18(2):116–140, 2001.
- [12] L. Dall’Amico, A. Barrat, and C. Cattuto. An embedding-based distance for temporal graphs. *Nature Communications*, 15:9954, 2024.
- [13] S. I. Dimitriadis et al. Tracking brain dynamics via time-dependent network analysis. *Journal of Neuroscience Methods*, 193(1):145–155, 2010.
- [14] N. Djurdjevac. *Methods for analyzing complex networks using random walker approaches*. PhD thesis, Fachbereich Mathematik und Informatik, Freie Universität Berlin, Germany, Apr 2012.
- [15] N. Djurdjevac Conrad, L. Helfmann, and J. et al. Zonker. Human mobility and innovation spreading in ancient times: a stochastic agent-based simulation approach. *EPJ Data Science*, 7(24), 2018.
- [16] G. Froyland, M. Kalia, and P. Koltai. Spectral clustering of time-evolving networks using the inflated dynamic Laplacian for graphs, 2024. Available at <https://arxiv.org/abs/2409.11984>.
- [17] Z. Gao et al. edge2vec: Representation learning using edge semantics for biomedical knowledge discovery. *BMC Bioinformatics*, 20:306, 2019.

- [18] M. Girvan and M. E. J. Newman. Community structure in social and biological networks. *Proceedings of the National Academy of Sciences*, 99(12):7821–7826, 2002.
- [19] S. Gómez, A. Díaz-Guilera, J. Gómez-Gardeñes, C. J. Pérez-Vicente, Y. Moreno, and A. Arenas. Diffusion dynamics on multiplex networks. *Physical Review Letters*, 110:028701, 2013.
- [20] C. Granell, R. K. Darst, A. Arenas, S. Fortunato, and S. Gómez. Benchmark model to assess community structure in evolving networks. *Phys. Rev. E*, 92:012805, Jul 2015.
- [21] D. Greene, D. Doyle, and P. Cunningham. Tracking the evolution of communities in dynamic social networks. In *Proceedings - 2010 International Conference on Advances in Social Network Analysis and Mining, ASONAM 2010*, volume 2010, pages 176–183, 08 2010.
- [22] A. Grover and J. Leskovec. node2vec: Scalable feature learning for networks. In *Proceedings of the 22nd ACM SIGKDD International Conference on Knowledge Discovery and Data Mining, KDD '16*, page 855–864, New York, NY, USA, 2016. Association for Computing Machinery.
- [23] L. Helfmann, N. Djurdjevac Conrad, P. Lorenz-Spreen, and C. Schütte. Modelling opinion dynamics under the impact of influencer and media strategies. *Scientific Reports*, 13:Article number: 19375, 2023.
- [24] L. Helfmann, N. Djurdjevac Conrad, P. Lorenz-Spreen, and C. Schütte. Supplementary code for the paper modelling opinion dynamics under the impact of influencer and media strategies, 2023. Supplementary code available at <https://doi.org/10.12752/9267>.
- [25] P. Holme and J. Saramäki. Temporal networks. *Physics Reports*, 519(3):97–125, October 2012.
- [26] A. Hsiao, A. M. S. Ahmed, S. Subramanian, N. Griffin, L. Drewry, W. Petri, R. Haque, T. Ahmed, and J. Gordon. Members of the human gut microbiota involved in recovery from vibrio cholera infection. *Nature*, 515, 09 2014.
- [27] X. Huang, D. Chen, and T. et al. Ren. A survey of community detection methods in multilayer networks. *Data Mining and Knowledge Discovery*, 35:1–45, 2021.
- [28] R. Humphries, K. Mulchrone, J. Tratalos, S. J. More, and P. Hövel. A systematic framework of modelling epidemics on temporal networks. *Applied Network Science*, 6(1):23, 2021.
- [29] A. Kirman. The economy as an evolving network. *Journal of Evolutionary Economics*, 7(4):339–353, 1997.
- [30] S. Klus and N. Djurdjevac Conrad. Dynamical systems and complex networks: A koopman operator perspective, 2024. Available at <https://arxiv.org/abs/2405.08940>.
- [31] S. Klus and N. Djurdjevac Conrad. Koopman-based spectral clustering of directed and time-evolving graphs. *Journal of Nonlinear Science*, 33(1):8, Nov 2022.
- [32] Habermann Lab. Phasik: Tools for phase-based analysis of time-series data. https://gitlab.com/habermann_lab/phasik, 2023. Accessed: 2024-08-02.
- [33] R. Lambiotte and M. T. Schaub. *Modularity and Dynamics on Complex Networks*. Cambridge University Press, 2022.
- [34] A. Lancichinetti and S. Fortunato. Benchmarks for testing community detection algorithms on directed and weighted graphs with overlapping communities. *Phys. Rev. E*, 80:016118, Jul 2009.

- [35] A. Lancichinetti, S. Fortunato, and F. Radicchi. Benchmark graphs for testing community detection algorithms. *Phys. Rev. E*, 78:046110, Oct 2008.
- [36] Y. Lin, Y. Chi, S. Zhu, H. Sundaram, and B. L. Tseng. Facetnet: a framework for analyzing communities and their evolutions in dynamic networks. In *The Web Conference*, 2008.
- [37] A. Longa, G. Cencetti, S. Lehmann, A. Passerini, and B. Lepri. Generating fine-grained surrogate temporal networks. *Communications Physics*, 7:22, 2024.
- [38] M. Lucas, A. Morris, A. Townsend-Teague, L. Tichit, B. Habermann, and A. Barrat. Inferring cell cycle phases from a partially temporal network of protein interactions. *Cell Reports Methods*, 3(2):100397, Feb 2023.
- [39] S. Mahdavi, S. Khoshraftar, and A. An. dynnode2vec: Scalable dynamic network embedding. *2018 IEEE International Conference on Big Data (Big Data)*, pages 3762–3765, 2018.
- [40] N. Masuda and P. Holme. Detecting sequences of system states in temporal networks. *Scientific Reports*, 9:795, 2019.
- [41] K. Melnyk. graphKKE: Library for the analysis of time-evolving graphs. <https://github.com/k-melnyk/graphKKE>, 2020. Accessed: 2024-08-02.
- [42] K. Melnyk. deep-metastability: Understanding microbiome dynamics via interpretable graph representation learning. <https://github.com/k-melnyk/deep-metastability>, 2023. Accessed: 2024-08-02.
- [43] K. Melnyk, S. Klus, G. Montavon, and T. O. F. Conrad. GraphKKE: graph kernel Koopman embedding for human microbiome analysis. *Applied Network Science*, 5(1), December 2020.
- [44] K. Melnyk, K. Weimann, and T. Conrad. Understanding microbiome dynamics via interpretable graph representation learning. *Scientific Reports*, 13:2058, 2023.
- [45] T. Mikolov, K. Chen, G. Corrado, and J. Dean. Efficient estimation of word representations in vector space, 2013.
- [46] M. Newman and M. Girvan. Finding and evaluating community structure in networks. *Physical review. E, Statistical, nonlinear, and soft matter physics*, 69:026113, 03 2004.
- [47] M. E. J. Newman. *Networks: an introduction*. Oxford University Press, Oxford; New York, 2010.
- [48] H. Owhadi and G. R. Yoo. Kernel flows: From learning kernels from data into the abyss. *Journal of Computational Physics*, 389:22–47, 2019.
- [49] C. Padilla-Iglesias, L. M. Atmore, J. Olivero, K. Lupo, A. Manica, E. Arango Isaza, L. Vinicius, and A. B. Migliano. Population interconnectivity over the past 120,000 years explains distribution and diversity of central african hunter-gatherers. *Proceedings of the National Academy of Sciences of the United States of America*, 119(e2113936119), 2022.
- [50] L. Peel and A. Clauset. Detecting change points in the large-scale structure of evolving networks. In *AAAI Conference on Artificial Intelligence*, 2014.
- [51] L. Peel, D. B. Larremore, and A. Clauset. The ground truth about metadata and community detection in networks. *Science Advances*, 3(e1602548), 2017.

- [52] B. Perozzi, R. Al-Rfou, and S. Skiena. Deepwalk: online learning of social representations. In *Proceedings of the 20th ACM SIGKDD International Conference on Knowledge Discovery and Data Mining*, KDD '14, page 701–710, New York, NY, USA, 2014. Association for Computing Machinery.
- [53] G. Rossetti. Graph benchmark handling community dynamics. *Journal of Complex Networks*, 5(6):893–912, 07 2017.
- [54] G. Rossetti and R. Cazabet. Community discovery in dynamic networks: a survey. *ACM Computing Surveys (CSUR)*, 51(2):35, 2018.
- [55] H. Sanhedrai and S. Havlin. Epidemics on evolving networks with varying degrees. *New Journal of Physics*, 24(5):053002, 2022.
- [56] M. Sarich, N. Djurdjevac Conrad, S. Bruckner, T. O. F. Conrad, and C. Schütte. Modularity revisited: A novel dynamics-based concept for decomposing complex networks. *Journal of Computational Dynamics*, 1(1):191–212, 2014.
- [57] C. Schütte and M. Sarich. *Metastability and Markov State Models in Molecular Dynamics: Modeling, Analysis, Algorithmic Approaches*, volume 24 of *Courant Lecture Notes*. American Mathematical Society in cooperation with the Courant Institute of Mathematical Sciences at New York University, 2013.
- [58] A. Sikorski, M. Weber, and C. Schütte. The augmented jump chain. *Advanced Theory and Simulations*, 4(4):2000274, 2021.
- [59] M. Trower, N. Djurdjevac Conrad, and S. Klus. Clustering time-evolving networks using the spatio-temporal graph Laplacian, 2024. Available at <https://arxiv.org/abs/2407.12864>.
- [60] A. van den Oord, Y. Li, and O. Vinyals. Representation learning with contrastive predictive coding. *CoRR*, abs/1807.03748, 2018.
- [61] U. von Luxburg. A tutorial on spectral clustering. *Statistics and Computing*, 17(4):395–416, 2007.
- [62] D. Watts and S. Strogatz. Collective dynamics of ‘small-world’ networks. *Nature*, 393:440–442, 1998.
- [63] J. Zonker, C. Padilla-Iglesias, and N. Djurdjevac Conrad. Insights into drivers of mobility and cultural dynamics of african hunter-gatherers over the past 120 000 years. *R. Soc. Open Sci.* 10: 230459, 2023.
- [64] J. Zonker, C. Padilla-Iglesias, and N. Djurdjevac Conrad. Supplementary code and data for Royal Society Open Science Manuscript rsos.230495, 2023. Supplementary code is available at <https://doi.org/10.12752/9254>.

Appendix

A Network Generator – Details

In the following, we detail our method for generating synthetic benchmark data using our new agent-based approach, as introduced in section 3.2.

A.1 Construction of the potential

We partition the time interval $[0, T]$ into $J \in \mathbb{N}^+$ subintervals I_j where $j = 1, \dots, J$. On each subinterval I_j we define a potential function U_j with $s(j)$ potential wells as

$$U_j(x, y) = \sum_{i=1}^{s(j)} c_{j,i} e^{-(m_{j,i}x+p_{j,i})^2 - (n_{j,i}y+q_{j,i})^2} + \frac{a_j x^2}{2} + \frac{b_j y^2}{2},$$

where $c_{j,i}, m_{j,i}, n_{j,i}, p_{j,i}, q_{j,i}$, for $i \in \{1, \dots, s(j)\}$ are adjustable parameters determining the depth, width, and position of the wells in the plane during the time-interval I_j , while the last two parameters a_j, b_j define the corrective component of the potential which serves to prevent particles from straying excessively from the wells due to the influence of noise coming from the stochasticity of the process. Note that by setting $m_{j,i} = 0$ or $n_{j,i} = 0$ we obtain degenerated "wells" which can serve as barriers between two half-planes parallel to y -axis or x -axis, respectively (Figure 6a). Since for each $t \in [0, T]$ there is a unique $1 \leq j(t) \leq J$ such that $t \in I_{j(t)}$ we define a time-dependent potential function as

$$U_t(x, y) = U_{j(t)}(x, y).$$

Remark A.1 *In what follows, we specify the choice of parameters for the potential functions used in the synthetic examples in Sections 3.4 and 3.5.*

Example Dataset: Community Split

The potential is computed using the following parameters. The left well, present during both phases ($j \in \{1, 2\}$), is characterized by $c_{j,1} = -5, p_{j,1} = 2, q_{j,1} = 0$ and $m_{j,1} = n_{j,1} = 1$. In Phase 1 ($j = 1$), the right well is specified with $c_{1,2} = -5, p_{1,2} = -2, q_{1,2} = 0$ and $m_{1,2} = n_{1,2} = 1$. During Phase 2 ($j = 2$), the right side features two wells defined by $c_{2,i} = -5, p_{2,i} = -1.8, m_{2,i} = n_{2,i} = 1$ for $i \in \{2, 3\}$ and $q_{2,2} = -2, q_{2,3} = 2$. Additionally, a barrier separating the left and right wells, present in both phases, is obtained by setting $c_{j,i} = 2, p_{j,i} = q_{j,i} = 0, m_{j,i} = 0$ and $n_{j,i} = 2$ for $j \in \{1, 2\}$ with i set dependent on the phase to match the total number of wells. Lastly, the corrective terms remain constant across both phases, with $a_j = b_j = 0.04$ for $j \in \{1, 2\}$.

Example Dataset: Community Hierarchy

The potential is computed using the following parameters. The depth parameter for all (non-degenerated) wells is uniformly set to $c_{j,i} = -5$. In Phase 1, the left well is positioned at $p_{1,1} = 2.5, q_{1,1} = 0$ while the right well is positioned at $p_{1,2} = -2.5, q_{1,2} = 0$. The width of both wells in this phase is defined by $m_{1,i} = n_{1,i} = 1$ for $i \in \{1, 2\}$. In Phase 2, the right well ($i = 3$) remains the same as in the previous phase, while the left side features two wells positioned at $p_{2,1} = 1.5, q_{2,1} = 1.2$ (lower well) and $p_{2,2} = 1.5, q_{2,2} = -1.2$ (upper well). The widths of these wells are specified by $m_{2,1} = m_{2,2} = 0.5$ and $n_{2,1} = n_{2,2} = 1$. In Phase 3, the two wells on the left side ($i = 1, 2$) persist,

while the right side now features two wells positioned at $p_{3,3} = -2, q_{3,3} = 1.8$ (lower well) and $p_{3,4} = -2, q_{3,4} = -1.8$ (upper well). The widths of these wells are given by $m_{3,i} = n_{3,i} = 0.7$ for $i \in \{3, 4\}$. Additionally, a barrier separating the left and right wells is present in all three phases. It is defined by setting $c_{j,i} = 2, p_{j,i} = q_{j,i} = 0, m_{j,i} = 1.3$ and $n_{j,i} = 0$ for $j \in \{1, 2, 3\}$ with i set dependent on the phase to match the total number of wells. Finally, the corrective terms remain constant throughout all phases, with $a_j = b_j = 0.04$ for $j \in \{1, 2, 3\}$.

Particle dynamics and snapshot construction

We now describe the the particle dynamics and how snapshots are constructed. Consider N particles moving through a 2-dimensional potential governed by the overdamped Langevin equation

$$dX_i(t) = -\nabla U_t(X_i(t)) dt + \sqrt{2\beta^{-1}} dW_i(t),$$

where $X_i(t)$ is position of the i th agent, β determines noise intensity, U_t is a time-dependent potential, and $W_i(t)$ is a standard Brownian motion [15]. Particles start at random positions within the plane and their trajectories are simulated using the Euler–Maruyama method over T/h steps, where h is the step size.

Snapshots of the temporal network are selected at intervals defined by a resolution parameter $r \in \mathbb{N}^+$ which provides control over the smoothness of the network dynamics. Alternatively, snapshots can aggregate over r -step windows, where proximity between nodes reflects their average distance over this period. For instance, in the example from Section 3.4, the positions of $N = 120$ particles are shown for five snapshots (see Figure 6c), corresponding to a total simulation of 150 steps ($\beta = 0.45, h = 0.05, r = 10$). This results in snapshots of the generated temporal network which correspond to the 10th to 150th time steps. Note that for now, the networks do not contains edges yet. We obtain 15, for the time being “edgeless”, networks that represent snapshots of our example benchmark. As long as the underlying potential of the dynamics remains constant, networks exhibit consistent community structures. In our example, the network transitions between two phases: the initial phase with two communities and the second phase where the right community splits into two. The snapshots reflect these changes, with the transition occurring in the 8th snapshot.

Edge Construction

Edges between nodes are added based on their spatial proximity. For each pair of nodes $u, v \in V$ in a snapshot α , the probability of an edge is determined by an evaluation function $f(d(u, v))$ where d denotes the Euclidean distance and f is given by:

$$f(x) = 1 - \xi \left(1 - \nu \left(\frac{1}{\pi} \tan^{-1}(\theta x - \omega) + \frac{1}{2} \right) \right)$$

with tunable parameters $\xi, \nu, \theta, \omega \in \mathbb{R}$. As shown in Figure 6b, the function ensures higher edge probabilities for closer nodes, forming communities around potential wells (here, we use $\xi = 1.015, \nu = 0.85, \theta = 5, \omega = 5$). The parameters θ and ω define the distance threshold for community formation, while ν and ξ control edge density within and between communities. For unweighted snapshot adjacency matrices, A_α are defined as $\mathbb{P}[A_\alpha(u, v) = 1] = f(d(u, v))$. In the weighted case, we use $w_\alpha(u, v) = f(d(u, v))$.

The full realization of an unweighted temporal network using this approach is shown in Figure 6d. Synthetic networks generated by this approach will serve as datasets for evaluating the performance and robustness of our method.